The Impact of Increased Recycle Content on Microstructure, Tensile Properties and Hemming Capability in Automotive Al-Mg-Si Alloys

by

Brian Thomas Kelley

B.S., Material Science and Engineering, The Pennsylvania State University, 2019

Submitted to the Graduate Faculty of the

Swanson School of Engineering in partial fulfillment

of the requirements for the degree of

Master of Science

University of Pittsburgh

2024

UNIVERSITY OF PITTSBURGH

SWANSON SCHOOL OF ENGINEERING

This thesis was presented

by

Brian Thomas Kelley

It was defended on

November 14, 2024

and approved by

Markus Chmielus, Ph.D., Associate Professor, Department of Mechanical Engineering & Materials Science

Ian Nettleship, Ph.D., Associate Professor, Department of Mechanical Engineering & Materials Science

Thesis Advisor: Zachary Harris, Ph.D., Assistant Professor, Department of Mechanical Engineering and Materials Science

The Impact of Increased Recycle Content on Microstructure, Tensile Properties and Hemming Capability in Automotive Al-Mg-Si Alloys

Brian Thomas Kelley

University of Pittsburgh, 2024

The following study investigated the impact of increased aluminum scrap utilization on the microstructure and mechanical properties of Al-Mg-Si alloys for use in automotive applications. Scrap-tolerant alloys represent a key developmental area as the automotive industry continues to strive for greater sustainability and lower cost. For the purposes of this study, a hypothetical scrap mixture, based on a projection from Ford F-150 post-consumer 6XXX (Al-Mg-Si) scrap, was used to derive three alloy compositions of interest. Each alloy targeted a base composition of Mg, Si, and Cu designed to meet Ford WSS-A175-A2 specification requirements, which is a grade commonly used in exposed applications requiring improved local formability for door hem operations. The three alloys targeted 0%, 33%, and 67% recycle content with Fe and Mn increasing as recycle content increased. To determine the impact of thermo-mechanical processing on the scrap tolerance of these alloys, each alloy was rolled to a final gauge of 1.0 mm, targeting cold reductions of 70%, 80% and 90%. Additionally, each alloy was heat treated using two separate practices, with the first targeting near the center of the Ford yield strength specification limits and the second targeting full dissolution of Mg_2Si.

Alloy microstructure was evaluated using optical metallography and scanning electron microscopy to identify and quantify observed phases. Additionally, electron backscatter diffraction was used to measure grain size. Tensile testing with measurement of plastic strain ratio was used

to evaluate mechanical properties associated with global formability. VDA bend testing and Ford flat hem testing was used to evaluate hemming capability.

Overall, this study found that moderate levels of scrap could be used to improve overall performance with appropriate thermomechanical processing modifications, as the local formability can be improved with increasing cold work without significant, negative impacts to tensile properties. However, higher levels of scrap were found to be exceedingly detrimental to global formability properties, likely hindering their general use for automotive applications. Future work is suggested to better understand how recycle content affects texture evolution during thermomechanical processing as such information could be leveraged to further refine processing strategies to increase the amount of allowable recycling content.

Table of Contents

1.0 Introduction **1**

1.1 Project Objective and Research Hypotheses **5**

1.2 Organization of Thesis **6**

2.0 Methodology **7**

2.1 Alloy Composition **7**

2.2 Sheet Fabrication **14**

2.3 Solution Heat Treatment **17**

2.4 Mechanical Testing **20**

2.5 Microscopy and Characterization **28**

3.0 Results **33**

3.1 Microscopy and Characterization **33**

3.2 Tensile Testing **41**

3.3 Hem and VDA Bend Testing **48**

4.0 Discussion **53**

4.1 Microstructure **53**

4.2 Mechanical Testing **59**

5.0 Conclusions **66**

6.0 Future Work **69**

7.0 Bibliography **70**

List of Tables

Table 1: Ford F-150 Aluminum Alloy Mix with Allowed Composition Ranges [23] 7

Table 2: Maximum Composition by Weight of Scrap Streams and Primary Aluminum for Determining Experimental Alloy Composition 10

Table 3: Minimum composition by Weight of Silicon, Copper, and Magnesium as determined by Scrap Usage compared to AA6022 and Target of Experimental Alloys..... 12

Table 4: Final Target Compositions by Weight of Control and Experimental Alloys..... 13

Table 5: Ingot Hot Rolling Reduction Schedule..... 16

Table 6: Solution Heat Treatment Soak Durations for "Equivalent Strength" Samples.... 19

Table 7: Index of Sample Lot Numbers..... 20

Table 8: Detailed Rating Scale of Hem Performance with Assigned Numerical Values..... 26

Table 9: Mg_2Si Content of 70% and 90% Cold work, Equivalent Strength Samples of 6XX0, 6XX1, and 6XX2..... 37

Table 10: Constituent Particle Content of 70% and 90% Cold Work, Equivalent Strength Samples of 6XX0, 6XX1, and 6XX2 38

Table 11: Predicted and observed quantities of insoluble phases in 6XX0, 6XX1, and 6XX2. 54

Table 12: 6XX0, 6XX1 and 6XX2 vs Ford WSS-A175-A2 Specification Limits. Properties listed are the range of values from all cold work levels..... 60

List of Figures

Figure 1: Various hem geometries, including the "3t" rope hem common in early door/closure design and the "3t" flat hem that is common in modern vehicles. [21]. 2

Figure 2: Ingot Homogenization Thermal Trace 15

Figure 3: Yield Strength vs Solution Heat Treatment Time Plot for HT Regression Trial. 18

Figure 4: ASTM B557M 50mm Gauge Length r&n Tensile Specimen 21

Figure 5: Ford Flat Hem Down Flange Step 23

Figure 6: Ford Flat Hem Pre-Hem Step 24

Figure 7: Ford Flat Hem Test Final Step 24

Figure 8: Ford Flat Hem Rating Scale from 1 to 4 per Ford BB 115-01 25

Figure 9: Schematic of VDA Bend Test Performed on 6XX0, 6XX1, and 6XX2 Samples .. 27

Figure 10: 100X Optical Micrograph of L-ST Plane of 6XX0-T4, 80% CW in As-Polished Condition (top) and Etched Condition (bottom) 29

Figure 11: 100X Optical Micrograph of L-ST Plane of 6XX0-T4, 80% CW in Electropolished and Anodized Condition 30

Figure 12: 1000X Electron Micrograph of L-ST Plane of 6XX0-T4, 70% CW 31

Figure 13: Representative inverse pole figure map of 6XX0-T4, 80% CW 32

Figure 14: 100X Optical Micrographs of As-Cast Samples of 6XX0, 6XX1, and 6XX2 in Etched Condition 34

Figure 15: 500X L-ST images at T/2 of F-temper Samples in As-Polished Condition. Scale Bars Indicate 50 μm. 35

Figure 16: 500X L-ST Images at T/2 in As-Polished Condition of Equivalent Strength Samples. Scale bars indicate 50 microns. Contrast increased 25% to improve particle visibility. 36

Figure 17: 100X L-ST Images at T/2 in Electro-polished and Anodized Condition of Equivalent Strength Samples. Scale bars indicate 200 □m. 39

Figure 18: Number-Weighted Average Grain Size of "Equivalent Strength" Lots as measured by Electron Backscatter Diffraction. Error Bars Reflect Number Weighted Grain Size Standard Deviation 40

Figure 19: Yield Strength Natural Aging Curves of "Equivalent Strength" Lots in L and LT Directions. Ford Specification Limit Indicated by the Dashed Lines. 42

Figure 20: Yield Strength Natural Aging Curves of "Peak Strength" Lots in L and LT Directions. Ford Specification Limit Indicated by the Dashed Lines. 43

Figure 21: Tensile Strength Natural Aging Curves of "Equivalent Strength" Lots in L and LT Directions. Ford Specification Limit Marked by Dashed Lines. 44

Figure 22: Tensile Strength Natural Aging Curves of "Peak Strength" Lots in L and LT Directions. Ford Specification Limit Marked by Dashed Lines. 44

Figure 23: Average Uniform Elong. by Lot and Direction. Ford Spec. Marked by Dashed Line. 45

Figure 24: Average Total Elongation by Lot and Direction. 46

Figure 25: Average r-value (plastic strain ratio) @ 10% Elongation by Lot and Direction. Ford Specification Limit Marked by Dashed Line. 47

Figure 26: Average n-value (strain hardening exponent) from 10% to 20% Elongation by Lot and Direction. Ford Specification Limit Marked by Dashed Line. 48

Figure 27: Flat Hem Simulation Results for each lot at 30 Days, 90 Days, and 180 Days Natural Age. Labeled Direction Indicated direction in which samples were cut. Ford Specification Limits marked by Dashed Line. 50

Figure 28: Flat Hem Simulation Sample Images of Equivalent Strength Lots, Tested at 30 Days, 90 Days, and 180 Days of Natural Age. Samples were cut in Longitudinal Direction..... 51

Figure 29: VDA Bend Test Results of Equivalent Strength Samples, Tested at 30 Days, 90 Days, and 150 Days of Natural Age. Labeled Direction indicates the direction in which were cut. 52

Figure 30: Constituent Particle Area Fraction, Particle Radius, and Number Density vs. Total Fe and Mn Content of 70% and 90% Cold Work Samples of 6XX0, 6XX1, and 6XX2. Error Bars Mark Particle Size Standard Deviation. 55

Figure 31: Constituent Particle Area Fraction vs. separated Fe, Mn Content of 70% and 90% Cold Work Samples of 6XX0, 6XX1, and 6XX2 55

Figure 32: Magnified SEM Image of 6XX2 with α Dispersoid and Constituent Phases Labeled..... 56

Figure 33: Number Weighted Grain size vs. Combined Fe and Mn content by Cold work Percentage..... 57

Figure 34: Uniform Elongation and Total Elongation of Equivalent Strength Lots Showing Large Impact of Increased Scrap Usage on Total Elongation..... 61

Figure 35: L and LT Stress Strain curves from Equivalent Strength Lots with OGL failure of E3370 LT Specimen..... 62

1.0 Introduction

The true start of the trend of mass aluminization of automobiles began in the mid-to-late 1980s with the Mazda RX-7 in 1985 and Acura NSX in 1989 [1]. Both vehicles were made with a mix of mostly 5XXX (Al-Mg) and 6XXX (Al-Mg-Si) series aluminum. 5XXX panels were used for applications requiring global formability, such as door inner panels, which must be stamped in a manner to provide space for electronics, airbags, and insulation. Conversely, 6XXX panels were used for applications requiring local formability and surface quality, such as body side and door outer panels, whose edges are tightly hemmed around the inner panels to seal the panels together. Additionally, high copper 6XXX (Al-Mg-Si-Cu) were used for components requiring higher strength, such as reinforcements and the vehicle frame [3]. Twenty years later, a similar blueprint was used when the Ford F-series trucks made the switch to an all-aluminum body, solidifying the widespread use of aluminum in the automotive industry.

The first generation of aluminum alloys used in automobiles was adapted from similar alloys employed in aircraft, building materials, and packaging. These alloys included 6XXX alloys, such as AA6022 and AA6111, for use in both structural and exposed applications. Such early automotive alloys had satisfactory global formability and excellent elongation; however, since many of these alloys had been developed for more general use, they lacked the local formability requirements required for sharp corners and bends [1]. Hems were particularly challenging, requiring exceptional ductility and fracture toughness to avoiding cracking during the hemming operation [6]. Though many steel alloys could perform a “3t” flat hem, shown below in **Figure 1**, door and body side designs often had to be modified to accommodate the limited bendability of

early aluminum alloys. These design accommodations can be clearly observed on cars from the 1990s and 2000s, which often exhibit smooth and streamlined panels with few corners and heavily utilization of the “3t” rope hems pictured below.

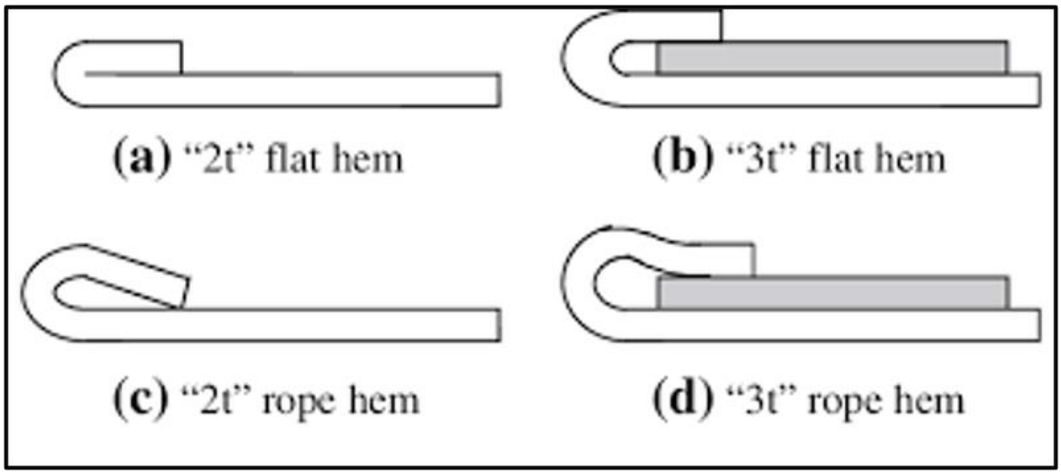

Figure 1: Various hem geometries, including the "3t" rope hem common in early door/closure design and the "3t" flat hem that is common in modern vehicles. [21]

As automotive aluminum technology has improved, alloys and processing methods have been developed to improve global and local formability. Today’s hemming grades utilize high levels of cold work to promote a fine grain structure and generally contain lower magnesium and silicon content to keep strength low for improved local formability. Such improvements have allowed for the more aggressive car styling and flat door hems that are commonplace in today’s automotive market. Though the attractiveness of modern designs is certainly subjective, the local formability improvements associated with tighter door hems alone can decrease the weight of a vehicle by several kilograms, while providing a superior seal between door inner and outer panels. Therefore, it is anticipated that the demands of modern vehicle design will result in local and global formality requirements becoming even more stringent as automotive OEMs (original equipment

manufacturers) seek to further eliminate material waste, trim excessive weight from cars, and increase design flexibility.

In addition to improving alloy formability for automotive applications, there has also been an increased focus on recycling and scrap usage in recent years, with many OEMs beginning to incorporate scrap usage targets into their alloy specifications. The primary drivers of this are cost and energy usage [20], as the refinement of pure aluminum, also known as primary aluminum, accounts for ~92% of the energy requirements of aluminum sheet production and requires 20-fold more energy than creating the same alloy via recycling of aluminum scrap. With roughly 80 percent of primary aluminum cost coming from the energy associated with refinement, aluminum scrap provides a significant cost savings opportunity for OEMs, aluminum suppliers, and consumers alike [4,14]. However, while the use of scrap in aluminum product has clear economic benefits, implementation is complicated by the strong sensitivity of aluminum alloys to the impurities and contaminants commonly found in scrap streams. For example, in the case of 6XXX-series aluminum alloys produced with scrap, iron and manganese levels are often increased. Iron is particularly common due to relatively high levels of iron oxides in aluminum ores and the heavy prevalence of steel in processing equipment. Conversely, manganese largely comes from mixing scrap with other alloys such as 3XXX-series and 5XXX-series aluminum alloys.

That challenges associated with these (and other) impurities is their effect on the alloy microstructure and properties. For example, both iron and manganese form phases, such as $Al_{12}(Fe,Mn)_3Si$ (α-phase) and Al_9Fe_2Si (β-phase), that are soluble in liquid aluminum, but have virtually no solubility in the solid aluminum matrix. This results in the formation of constituent particles during solidification [8]. The particles are thought to have mostly negative impacts on

material properties. Notably, the α and β phase particles consume silicon, reducing the amount of available Mg_2Si and subsequently, the extent of solution and precipitation hardening. The particles are also quite brittle, which can cause a decrease in alloy fracture toughness and ductility [8]. However, some characteristics of these particles can be beneficial for very specific applications that require improved local formability. Since the particles are insoluble, they can promote particle-stimulated nucleation of grains, leading to a smaller average grain size [12], which is known to lower the likelihood of crack nucleation during bending operations. Additionally, the reduction in strengthen due to the formation of these particles can improve local formability due to the inverse relationship between strength and local formability.

Given the potential for detrimental effects from impurities, the value of aluminum alloy scrap decreases drastically as contaminant concentrations increase or if alloy series are mixed. Scrap can largely be categorized as either pre-consumer or post-consumer scrap. Pre-consumer scrap typically comes from trimming, blanking, and stamping, is often segregated by series, and is generally returned directly to suppliers from OEMs [23]. This form of scrap is of generally high purity, with compositional variation driven by the variability within the given aluminum alloy series. Conversely, post-consumer scrap comes from scrapping whole vehicles and is often heavily contaminated, in addition to containing a mix of multiple aluminum alloy series. Fortunately, recent improvements in scrap sorting methods, such as laser induced breakdown spectroscopy, have allowed for post-consumer scrap to be sorted by alloy series at scale, though issues with contamination remain [19]. Because of this, post-consumer scrap is often significantly cheaper than pre-consumer scrap and can only be used as a small percentage of the total scrap usage in new aluminum coils. For this reason, high recycle alloys, which are alloys that can tolerate high levels

of scrap usage and contaminant content without detrimental reductions to product formability, are being pursued by OEMs and aluminum suppliers alike.

1.1 Project Objective and Research Hypotheses

The primary objective of this study is to elucidate the effect of increased recycle content on microstructure and mechanical properties in wrought Al-Mg-Si alloys and understand whether changes in thermomechanical processing schedules can improve the scrap tolerance of these alloys. The increased use of recycle content, and the corresponding increase in alloy Fe and Mn content, is generally expected to have negative impacts on tensile properties and bendability. However, the addition of these elements as well as increasing the extent of cold-work level is also expected to yield a finer grain size that may have a positive impact on alloy bendability. Thus, the following study attempted to prove that when targeting comparable strength, moderate levels of recycle content will improve product bendability across various cold reduction levels, while high levels of recycle content are likely to lead to decreased bend performance vs. control samples across all cold reduction levels. Based on these expectations and governing objectives, this research project sought to evaluate the following research hypotheses:

1. Increasing the amount of recycled scrap utilization will increase the volume fraction of constituent phases, resulting in a reduction in global ductility properties, such as elongation to failure, below the Ford specification for the highest recycle content alloy.
2. Increasing the extent of cold work for a given scrap utilization level will improve the local formability properties, such as hem-ability.

3. Increasing volume fraction of constituent phases will result in particle stimulated nucleation in addition to decreased ductility. Moderate levels of scrap utilization will result in improved hem performance due to the decreased grain size.
4. High levels of scrap utilization will result in decreased hem performance as the decreased ductility will outweigh the benefits of decreased grain size.

1.2 Organization of Thesis

To assess these research hypotheses, this thesis is organized as follows. Chapter 2 provides an overview of the different automotive aluminum alloys and thermomechanical processing approaches used in this study and provides details for the methods and analyses employed to characterize alloy microstructural parameters, uniaxial tensile properties, and formability. The results of these experiments are reported in Chapter 3 and then discussed in the context of the preceding research objectives and hypotheses in Chapter 4. The conclusions of the thesis and potential future research directions for further exploration are then provided in Chapters 5 and 6, respectively.

2.0 Methodology

2.1 Alloy Composition

Processing and test methods were selected to determine the impact on aluminum alloy grades intended for use in exposed automotive applications that require hemming operations. When discussing aluminum usage in the automotive industry, the first vehicle to come to mind is the Ford F-150. This truck has been the best-selling vehicle in the United States for nearly 50 years, with 750,000 units sold in 2023 [13]. Since 2014, the body and closures of this vehicle have been made entirely from aluminum alloys. As one might expect, this creates a potential for substantial amounts of scrap through the end of life of each vehicle, making it critical to understand the types of aluminum present and develop a general strategy for recycling. Because of this, the F-150 will serve as the source of a hypothetical scrap mix for the purposes of this study.

Table 1: Ford F-150 Aluminum Alloy Mix with Allowed Composition Ranges [23]

	Kg/Vehicle	Cu (wt.%)	Si(wt.%)	Fe(wt.%)	Mn(wt.%)	Mg(wt.%)
Low Cu 6XXX	92.6	≤0.20	0.50-1.00	≤0.30	≤0.15	0.40-0.80
High Cu 6XXX	95.2	0.50-0.80	0.55-0.95	≤0.30	≤0.30	0.55-0.95
Low Mg 5XXX	31.4	≤0.10	≤0.25	≤0.35	≤0.5	2.90-3.50
High Mg 5XXX	19.7	≤0.10	≤0.20	≤0.35	0.20-0.50	4.20-5.00

As outlined in **Table 1**, the aluminum alloys found in a representative Ford F-150 can be broken down into four main categories: high magnesium 5XXX, low magnesium 5XXX, high

copper 6XXX, and low copper 6XXX. The 5XXX series alloys make up roughly 20% of total aluminum mass and are used for the floor, inner door panels, and select reinforcement brackets through the structure of the vehicle [23]. The high copper 6XXX series alloys, like AA6111, make up approximately 40% of the aluminum mass in each F-150. These alloys are primarily strengthened by the addition of solute magnesium and silicon as well as through the formation of a precipitate phase, β-Mg_2Si [9]. The presence of copper contributes additional strengthening through solid solution strengthening and precipitation hardening of Q'-phase precipitate (Al-Cu-Si-Mg) [15]. Per the governing Ford WSS-M2A175-A2 specification, high copper 6XXX grades have yield strengths between 125-195 MPa, tensile strengths of 220-300 MPa, and uniform elongations of >19% [18]. These alloys are used to construct the "Body in White," or the structural components of the body due to their excellent strength; example parts include B-pillars, crossmembers, and reinforcements. Unfortunately, the copper in these alloys increases their susceptibility to filiform corrosion, making them unsuitable for use in exposed parts [7]. Because these grades are expected to have high strength, they often contain more silicon and magnesium than low copper 6XXX grades; they also tend to have higher levels of iron and manganese since they do not have required levels of hemming performance. As such, these compositional ranges allow high copper 6XXX to be very scrap tolerant, but the increased levels of copper, iron and manganese contents subsequently limit the ability of other alloys to absorb its scrap.

The low copper 6XXX series alloys, like AA6022, are used in components that are exposed as well as those that are hemmed. These alloys are lower strength and typically rolled to thinner gauges, 0.8-1.2 mm, to facilitate hemming and improve surface finish [10]. The lower copper levels allow for excellent corrosion resistance while the low strength and iron/manganese levels facilitate superior hem-ability; parts made from low copper 6XXX need to be strong enough to

resist dents but are rarely used in structural applications. As a result of their higher purity, low copper 6XXX series alloys are often very easy to recycle into solute-richer alloys, such as higher copper 6XXX grades, but are not very accepting of scrap. As the push for recyclability in the automotive aluminum industry increases, low copper 6XXX alloys are the primary focus of high recycle development efforts. The goal of such development efforts is ultimately to find processing methods or compositions that can maintain excellent local formability and corrosion resistance, while accommodating higher levels of common contaminants [5].

This study will be focusing on meeting the T4 properties of the WSS-M2A174-A2 specification, or the Ford dent-resistant grade of low copper 6XXX aluminum alloy. This grade has slightly higher strength and less stringent hemming requirements than enhanced hemming grades, with only 7% pre-strain required before performing the hem. This grade is required to meet a yield strength range of 105-145 MPa, tensile strength range of 200-270 MPa, uniform elongation of 19%, and plastic strain ratio (r-value) of 0.5 between 30-90 days natural age. This grade is also expected to perform a flat hem without cracking up to 90 days after heat treatment (i.e., at 90 days of natural aging) [16].

To constrain the number of variables in this study, a hypothetical scrap composition was used that is based on a general mix of Ford 6XXX series alloys from the Ford F-150. Because the F-150 contains roughly equivalent weights of high copper and low copper 6XXX alloys, the hypothetical scrap mix is assumed to be 50-50. In manufacturing, scrap compositions are highly variable due to an ever-changing mix of alloy ratios and contamination, which results in scrap often being sold according to composition ranges. Casters, in turn, typically assume the scrap contains the maximum allowable levels of every element except aluminum, which prevents the

casting of ingots that exceed operating limits and would therefore require scrapping. The maximum compositions for these scrap streams, shown below in **Table 2**, were averaged with an additional 0.2 wt.% iron added to reflect contamination from steel rivets, shredding tools, storage containers, etc. The target "scrap" composition below was then mixed with P1020 primary aluminum to derive the alloy compositions for the 33% scrap and 67% scrap alloys, with a primary focus on the manganese and iron levels.

Table 2: Maximum Composition by Weight of Scrap Streams and Primary Aluminum for Determining Experimental Alloy Composition

Element	Ford High Copper Scrap	Ford Low Copper Scrap	Overall Scrap	P1020 Aluminum
	Max Composition by Weight (%)			
Silicon, Si	0.95	1.00	0.98	0.10
Iron, Fe	0.30	0.30	0.50	0.20
Copper, Cu	0.80	0.20	0.50	0.03
Manganese, Mn	0.30	0.15	0.23	0.02
Magnesium, Mg	0.95	0.80	0.88	0.03
Chromium, Cr	0.10	0.10	0.10	0.02
Zinc, Zn	0.10	0.10	0.10	0.03
Titanium, Ti	0.10	0.10	0.10	0.02

Once the composition of scrap was determined, setting the composition of the three test alloys to be evaluated in this thesis was straightforward. Beginning with the control alloy (6XX0) iron and manganese levels were set in the center of the AA6022 composition limits: 0.125 wt.% and 0.060 wt.%, respectively. The control alloy, largely based on AA6022, is representative of high purity alloys that are widely employed for aluminum closures since the release of the 2015 F-150. This alloy is expected to perform a hemming operation without cracking through 90 days of natural aging, as is typical with other 6XXX series alloys used in outer closure panels. The 33%

scrap utilization alloy (6XX1) has elevated levels of iron and manganese, set at 0.30 wt.% and 0.09 wt.%, respectively. Though both iron and manganese contents are far above the levels allowed in AA6022, this alloy does fall within the allowable compositional ranges of Ford low copper 6XXX-series alloys. Finally, the 67% scrap utilization alloy represents a stretch target for iron and manganese content, targeting 0.40 wt.% Fe and 0.157 wt.% Mn. This final alloy would be considered unallowable under current requirements, as these compositions fall outside of the iron and manganese limits allowed by Ford for outer closure panels.

Though scrap utilization was varied across the three test alloys, target compositions were fixed for all elements aside from iron and manganese to simplify the number of variables considered. As such, there are a few notable elements where the concentrations deviated from those that would be present if the set percentage of scrap were utilized; these elements are shown in **Table 3**, while **Table 4** provides the final compositions of each tested alloy. As with all grades used in hemming applications, the alloys evaluated in this study targeted relatively low strength, with specific emphasis on achieving a T4 strength capable of meeting Ford WSS-M2A174-A2 specification requirements. Because of this, both magnesium and silicon content are expected to be relatively low. Targeted silicon levels were therefore set at 0.80 wt.%, which matches the minimum silicon composition limits of AA6022 [15]. Magnesium levels were set at 0.595 wt. % for all alloys, equivalent to the minimum composition for an alloy with 67% scrap utilization. In the case of both Mg and Si, these compositional targets fall close to the middle of acceptable Ford low copper 6XXX composition ranges. With the incorporation of high copper scrap, and the assumption that copper content was equal to the maximum limit, copper would quickly exceed the 0.2 wt.% limit set by car manufacturers for use in exposed parts if the actual values (**Table 3**) expected from incorporating scrap were used. However, unlike iron and manganese limits where

OEMs may be flexible, it is highly unlikely that copper limits would be increased due to concerns over corrosion susceptibility. Additionally, with the cost of copper being particularly high, it is likely that any scrap purchased would not contain the maximum allowable copper content. Therefore, the copper content for all three alloys was set at 0.185 wt.% to match the copper content of the 33% scrap utilization alloy. Finally, because of the expense of additional Cr, Zn, and Ti, as well as the potential for unknown cross effects, these three elements were negated from the study and all alloys targeted the maximum level of these elements found in P1020. Final compositions for the three tested alloys are shown below with 6XX0 representing the control, 6XX1 representing the 33% scrap utilization alloy, and 6XX2 representing the 67% scrap utilization alloy.

Table 3: Minimum composition by Weight of Silicon, Copper, and Magnesium as determined by Scrap Usage compared to AA6022 and Target of Experimental Alloys

Element	AA6022		33% Scrap Alloy	67% Scrap Alloy	Study Target
	Max wt.%	Min Wt.%	Min wt.%	Min wt.%	wt.%
Silicon, Si	0.8	1.5	0.39	0.69	0.8
Copper, Cu	0.01	0.11	0.19	0.34	0.19
Magnesium, Mg	0.45	0.7	0.31	0.60	0.6

Table 4: Final Target Compositions by Weight of Control and Experimental Alloys

Element	6XX0	6XX1	6XX2
	Target Composition by Weight (%)		
Silicon, Si	0.80	0.80	0.80
Iron, Fe	0.13	0.30	0.40
Copper, Cu	0.19	0.19	0.19
Manganese, Mn	0.07	0.09	0.16
Magnesium, Mg	0.60	0.60	0.60
Chromium, Cr	0.03	0.03	0.03
Zinc, Zn	0.03	0.03	0.03
Titanium, Ti	0.02	0.02	0.02

With the goal of meeting WSS-M2A174-A2 specification requirements, each alloy would need to be processed in a fashion that allowed it to remain within the range of tensile properties between 30- and 90-days of natural aging as well as pass the Ford flat hem test through 90 days of natural aging. To accomplish this, each alloy was rolled to 1.0 mm gauge with 70%, 80% and 90% reduction. The variation in cold mill reduction was performed to modify the range of grain sizes present in each of the samples to determine which grain size range would yield the best hemming performance. Additionally, to compensate for potential differences in strength due to grain size differences and constituent levels, each alloy was heat treated according to two methods. The first method targeted full dissolution of Mg_2Si and the maximum achievable strength of the alloy in the T4 temper, while the second method sought to achieve a targeted equivalent strength for all alloy-cold reduction combinations. Both methods will be detailed in subsequent sections.

2.2 Sheet Fabrication

One book mold measuring 15 cm x 45 cm x 125 cm was cast for each composition, with a total ingot weight of approximately 230 kg. After casting, ingots were scalped using a CNC mill, removing ~10 mm from the top and bottom edges of the ingots. This is done to remove the liquation enriched zone from the ingot as well as to ensure a consistent surface quality. The liquated region on the other faces is not removed at this point as it can be easily trimmed away upon completion of rolling. After scalping, all three ingots were stress relieved using a 12 h., 260 °C thermal cycle as a precautionary measure prior to further sawing of the ingots. Once cooled. the ingots were then divided into three sections, with each section reserved for one of the final cold work percentages of 70%, 80% and 90%.

Homogenization and rolling were conducted in a manner that reasonably simulates expected plant processing. In a true production scenario, ingots are much larger than those employed in this study, requiring longer heating and cooling cycles during the initial stages of production. To compensate for the size difference, the heat treatment laboratory ovens were set to follow temperature curves that approximate the heating rates seen by plant-scale ingots. Additionally, the rolling equipment used for plant-scale ingots is much more powerful than laboratory-scale equipment, which allows for larger reductions per pass. These two factors are the hardest to mimic during hot rolling in a laboratory setting, as (1) laboratory-scale hot rolling takes much longer to perform due to the lower reduction per pass and (2) laboratory-scale ingots cool more quickly. As such, to compensate for the faster cooling of smaller ingots and longer rolling practice, laboratory-scale ingots are typically reheated several times throughout rolling.

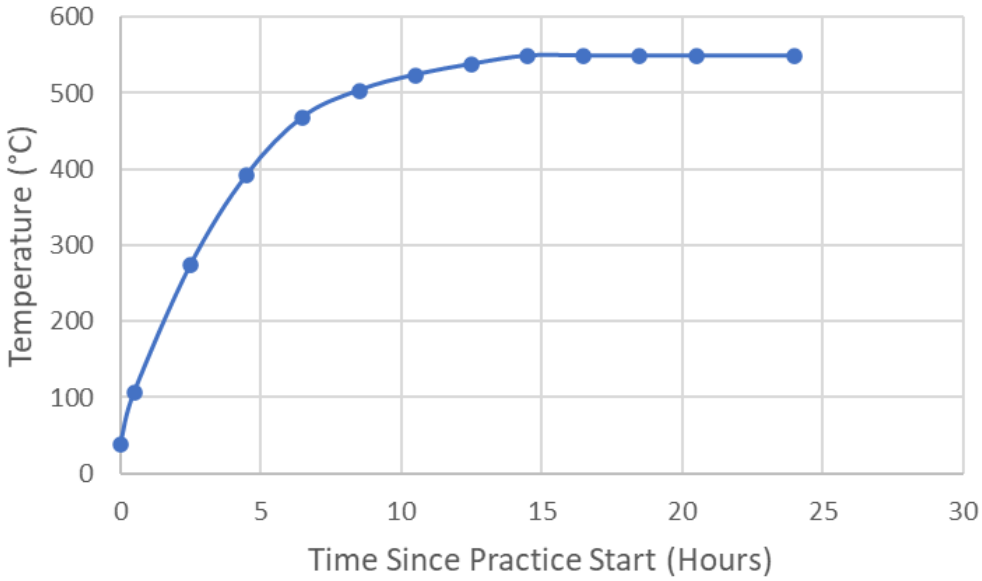

Figure 2: Ingot Homogenization Thermal Trace

Once the ingot sections were prepared, each ingot section was homogenized using the practice outlined in the thermal trace in **Figure 2**. This practice utilizes a 16-h. logarithmic heat up, followed by an 8-hr soak at 550 °C; this soak temperature was chosen by simulating the Mg_2Si solvus temperature in each of the three compositions using proprietary software. Immediately after the completing of the 8-h. soak, ingots were pulled from the furnace and rolled down from a thickness (i.e., gauge) of 150 mm to 50 mm. This process was completed in a total of 16 passes for each of the ingots in the temperature range of 530 °C to 400°C. Once rolled to 50 mm in gauge, each slab was placed back in the furnace for a 2-h. soak at 520°C. This was done to reheat the ingot for further hot rolling and re-homogenize after the relatively slow cooling of the ingot during the first phase of rolling.

Once the 2-h. soak was completed, the ingots went through four additional rolling passes, reaching a target gauge of 25.4 mm, while staying above 400 °C. After this point, a 400 °C reheat cycle with 1-h. soak was completed between each pass of the rolling mill until the final target

gauge was reached. **Table 5** below contains a full description of the rolling mill passes and reheat cycles. In keeping with industry terminology, gauge refers to the thickness of the sheet, while draft refers to the targeted reduction performed during the rolling mill pass. The thickness of the material after hot-rolling is referred to as the hot-band gauge. Depending on how thick the material is, it may be referred to as sheet or slab. Generally, items thicker than 6 mm are referred to as slab, while material thinner than 6 mm is referred to as sheet.

Table 5: Ingot Hot Rolling Reduction Schedule

Hot-Band Ga. (mm)	Final Gauge (mm)	Pass No.	0	1	2	3	4	5	6	7	8	9	10	11	12
0.131"	0.0394”	Gauge (mm)	50.8	44.5	38.1	31.8	25.4	22.2	19.1	15.9	12.7	9.5	6.4	4.8	3.3
		Draft (mm)	-	6.4	6.4	6.4	6.4	3.2	3.2	3.2	3.2	3.2	3.2	1.6	1.4
0.197"	0.0394”	Gauge (mm)	50.8	44.5	38.1	31.8	25.4	22.2	19.1	15.9	12.7	9.5	7.9	6.4	5.0
		Draft (mm)	-	6.4	6.4	6.4	6.4	3.2	3.2	3.2	3.2	3.2	1.6	1.6	1.3
0.394"	0.0394”	Gauge (mm)	50.8	44.5	38.1	31.8	25.4	22.2	19.1	17.5	15.9	14.3	12.7	11.1	10.0
		Draft (mm)	-	6.4	6.4	6.4	6.4	3.2	3.2	1.6	1.6	1.6	1.6	1.6	1.1

Once all ingots were rolled to the hot-band gauge, the metal was allowed to cool to room temperature in preparation for cold rolling. In each case, cold rolling was performed targeting 10% reduction with each pass until the final gauge was reached. Since this operation is performed near room temperature, any difference in the number of passes is expected to have minimal impact on final tensile properties.

2.3 Solution Heat Treatment

Because the variation in iron and manganese, as well as cold work level, can have significant impacts on strength, the decision was made to evaluate all alloys in conditions targeting both peak strength and equivalent strength. This necessitated the development of unique solution heat treatment practices for each alloy/cold work combination. To find the relationship between time in the furnace and yield strength, a trial was conducted in which samples of each alloy-cold work combination were heat treated for durations between one and four minutes in 30 second intervals using an oven set to 560°C. This temperature was chosen because it is slightly above the calculated Mg_2Si solvus temperature, but well below the calculated solidus temperature of the alloy. Samples were then air quenched with fans to minimize the risk of warping.

Once solution-treated, specimens were naturally aged for 10 days before tensile testing to capture the effect of the most rapid portion of natural aging and because this represents the timing of standard lot release testing. Samples were then evaluated according to the ASTM B557M standard for uniaxial tensile testing of wrought aluminum product. Results were then plotted as shown below in **Figure 3** to develop a regression model to predict the tensile yield strength (TYS); note that the points circled in **Figure 3** were excluded as outliers due to their anomalous departure from typical behavior.

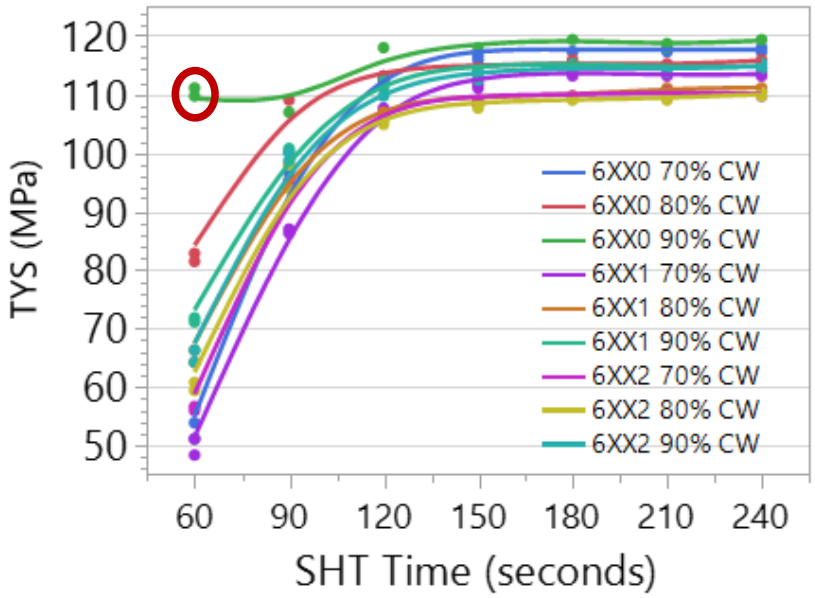

Figure 3: Yield Strength vs Solution Heat Treatment Time Plot for HT Regression Trial

The parameters included in the model were solution heat treatment duration, alloy composition, and cold work percentage, as these variables are expected to most strongly influence the TYS. Though targeting a natural age of 10 days at testing, samples were tested between natural ages of 9-12 days. Because of this, proprietary aging constants of similar products were used to normalize all data points to 10 days of natural aging. Examination of the data demonstrated that a 4th order polynomial relationship between solution heat treatment time and TYS with first order relationships between TYS and alloy/cold work percentage yielded the best fit. The predictive relationship determined from this evaluation is shown in Equation 1 below, along with the associated fitting parameter constants, where x is equal to solution heat treat duration in seconds.

$$TYS(MPa) = C01(x - C02)^4 + C03(x - C02)^3 + C04(x - C02)^2 + C05 * x + \begin{Bmatrix} XA58 & C06 \\ XA59 & C07 \\ XA60 & C08 \end{Bmatrix} + \begin{Bmatrix} 70\%CW & C09 \\ 80\%CW & C10 \\ 90\%CW & C11 \end{Bmatrix} + C12$$

C1 = -3.07E-7 C2=157.24 C3=2.87E-5 C4=-7.91E-5 C5=-1.80E-4 C6=3.59

C7=-1.36 C8=-2.23 C9=-3.51 C10=-0.18 C11=3.68 C12=112.54

(2-1)

After the predictive model was developed, 108 MPa in the long-transverse (LT) direction was chosen as the target strength for the "equivalent strength" condition. This strength level is near the middle of the Ford low copper 6XXX-series strength range and is within the achievable strength ranges for all alloy-cold work combinations in this study. Upon determining the target heat treatment times for all alloy-cold work combinations, lab furnaces were used to heat treat seven 30 cm x 30 cm sheets of each alloy-cold work combination for tensile and hem testing using the previously described methods and rapid air quenching via fans. The "equivalent strength" heat treatment durations for each alloy-cold roll combination are listed below in **Table 6**.

Table 6: Solution Heat Treatment Soak Durations for "Equivalent Strength" Samples

Alloy	Cold Work %	Heat treatment (hr:min:s)
6XX0 (Control)	70%	0:01:51
6XX0 (Control)	80%	0:01:42
6XX0 (Control)	90%	0:01:35
6XX1 (33% Scrap)	70%	0:03:05
6XX1 (33% Scrap)	80%	0:01:56
6XX1 (33% Scrap)	90%	0:01:45
6XX2 (67% Scrap)	70%	0:04:00
6XX2 (67% Scrap)	80%	0:02:00
6XX2 (67% Scrap)	90%	0:01:47

To accompany the equivalent strength samples, specimens from each alloy-cold work combination was also heat treated to its full-strength potential to enable an additional comparison and provide further insight regarding the impact of sample strength on hem performance with varying chemistry. The data from the heat treatment regression trial in **Figure 3** were used to design this practice, with the TYS versus solution heat treatment duration becoming flat for all alloys after durations of three to four minutes. To account for potential variation in oven

temperature and sample heating rates, all “full strength” samples were solution heat-treated for a duration of five minutes before being pulled and quenched with fans.

2.4 Mechanical Testing

A total of 18 different compositions-cold work-strength level combinations were evaluated for times between 0 and 6 months of natural aging; an index for the different alloys is shown in **Table 7** below.

Table 7: Index of Sample Lot Numbers

Lot Number	Alloy	Cold Reduction	Target Strength
E0070	6XX0 – 0% Scrap	70% CW	Equivalent
E0080	6XX0 – 0% Scrap	80% CW	Equivalent
E3390	6XX0 – 0% Scrap	90% CW	Equivalent
E3370	6XX1 – 33% Scrap	70% CW	Equivalent
E3380	6XX1 – 33% Scrap	80% CW	Equivalent
E3390	6XX1 – 33% Scrap	90% CW	Equivalent
E6770	6XX2 – 67% Scrap	70% CW	Equivalent
E6780	6XX2 – 67% Scrap	80% CW	Equivalent
E6790	6XX2 – 67% Scrap	90% CW	Equivalent
P0070	6XX0 – 0% Scrap	70% CW	Peak
P0080	6XX0 – 0% Scrap	80% CW	Peak
P3390	6XX0 – 0% Scrap	90% CW	Peak
P3370	6XX1 – 33% Scrap	70% CW	Peak
P3380	6XX1 – 33% Scrap	80% CW	Peak
P3390	6XX1 – 33% Scrap	90% CW	Peak
P6770	6XX2 – 67% Scrap	70% CW	Peak
P6780	6XX2 – 67% Scrap	80% CW	Peak
P6790	6XX2 – 67% Scrap	90% CW	Peak

The WSS-A174 specification was heavily referenced when determining the testing campaign for these specimens. In keeping with the requirements of the Ford 6DR grade, specimens were evaluated for tensile and formability properties through the maximum expected shelf life of 180 days. In typical cases, the material is expected to meet required properties through 90 days natural age; though fluctuations in demand may occasionally require older material to be used. However, material is typically scrapped after reaching 6 months of natural aging due to increased risk of failure during forming, therefore samples were not evaluated beyond this threshold.

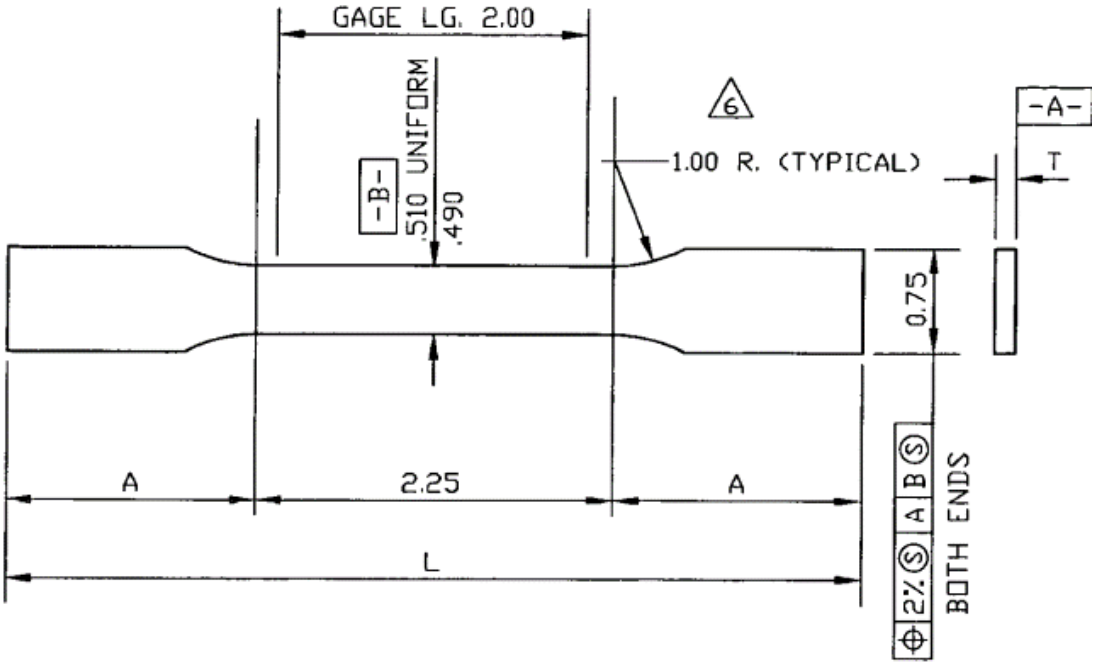

SPEC. NO.	T	L	A
1	.375–.500	11.0	4.37
2	.250–.375	10.5	4.13
3	< .250	9.0	3.37

Figure 4: ASTM B557M 50mm Gauge Length r&n Tensile Specimen

Uniaxial tensile properties were evaluated monthly through 6 months of natural age, with baseline testing performed at seven days of natural age. Experiments were performed using the standard ASTM B557M 50 mm gauge length “r&n” specimen. This specimen design is shown in **Figure 4** and allows for measurement of the plastic strain ratio (r), strain hardening exponent (n), and typical strength and elongation metrics. Duplicate samples were always tested in case of invalid tests caused by failures outside of the extensometer gage length or malfunctioning extensometers. Results were then screened for outliers using JMP statistical software.

The Ford flat hem test was utilized to assess the local formability of samples in a manner consistent with the Ford specification. All samples were evaluated at 1, 3, and 6 months of natural aging; the 1-month interval is indicative of a “best case scenario”, while the 3-month interval is indicative of material close to expiration age. The 6-month testing is performed to evaluate the longer-term aging performance of the material as well as assess the ability of each material to be used beyond the current specification-defined expiration date. The hem test utilizes a combination of stretching and bending to simulate the strain that a door hem may encounter when the pre-formed outer door panel is joined to the inner door panel. In keeping with the requirements of the Ford WSS-M174-A2 specification, samples were stretched to seven percent prior to testing. To facilitate efficient specimen preparation, the heat-treated sheet was sheared into 50mm x 300mm long coupons for stretching. These coupons were sheared both along and perpendicular to the rolling (L) direction, then stretched along the 300 mm axis. The stretched coupons were then machined into four rectangular specimens with a length of 57 mm and a width of 25.5 mm and deburred, per Ford specification BB 115-01: Flat Hem Test Procedure for Aluminum Alloy Sheet [17]. The use of four duplicate specimens for each sample is required by the Ford specification.

The Ford flat hem test is performed in a three-step process, where the first step is referred to as the 90° flanging, schematically shown in **Figure 5** below. During this step, the specimen is held in place while a moving die presses the specimen to a 90° bend. The stationary portion of the die utilizes an adjustable inner radius to set the bend radius of the hem. This radius is set to just below the nominal gauge of the samples to account for any thinning after stretching. In the case of the specimens for this study, the nominal gauge before stretching was 1.0 mm and was expected to be ~ 0.95 mm after stretching.

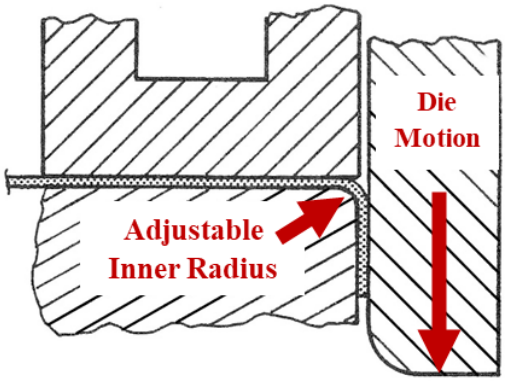

Figure 5: Ford Flat Hem Down Flange Step

After the down-flange step, the samples are flipped over and then undergo the second step of the hemming process, known as the 45° flanging and shown schematically in **Figure 6**. This step utilizes a lubricated, angled die to force the specimen from a 90° angle to a 45° angle (135° of total bend).

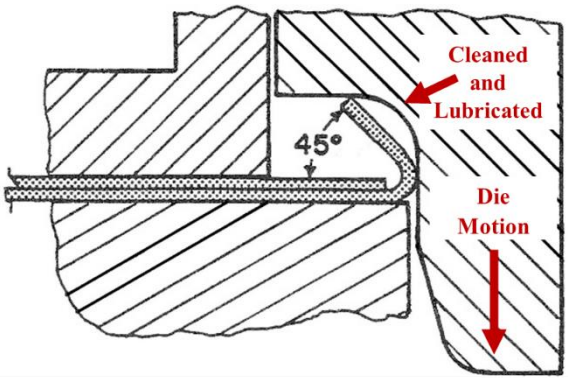

Figure 6: Ford Flat Hem Pre-Hem Step

Finally, samples are moved to the final station of the hemming process, often referred to as the flat hem and schematically shown in **Figure 7**, where the hems are pressed flat. This step creates the final shape of the bend and is often the portion of the forming operation that leads to cracking in materials with poor hem performance.

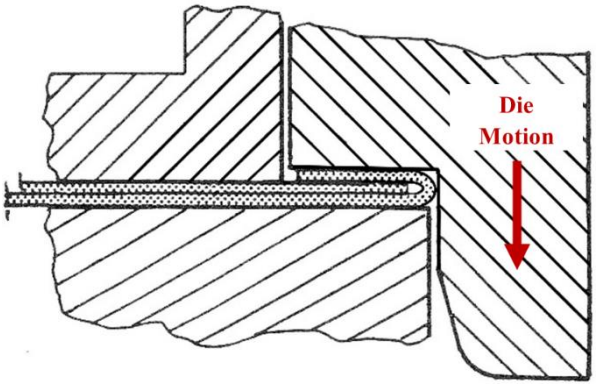

Figure 7: Ford Flat Hem Test Final Step

After the hemming test is completed, the folded edge of each sample is viewed under bright lights for a numerical rating of the hem quality. Samples are rated according to the Ford scale with ratings of between 1 and 4, where 1 represents an excellent hem and 4 represents a failed hem. Images of each rating are shown in **Figure 8** and are qualitatively described as follows by

Ford BB 115-01: “Acceptable; 1: No cracking, no to mild orange peel; 2: No cracking, mild to heavy orange peel. Not acceptable; 3: Crack initiation lines (i.e., lines of localized thinning or crazing) parallel to the bend line or discontinuous cracks parallel to bend line; 4: Continuous cracks or complete, through-thickness fracture.” (pg. 8).

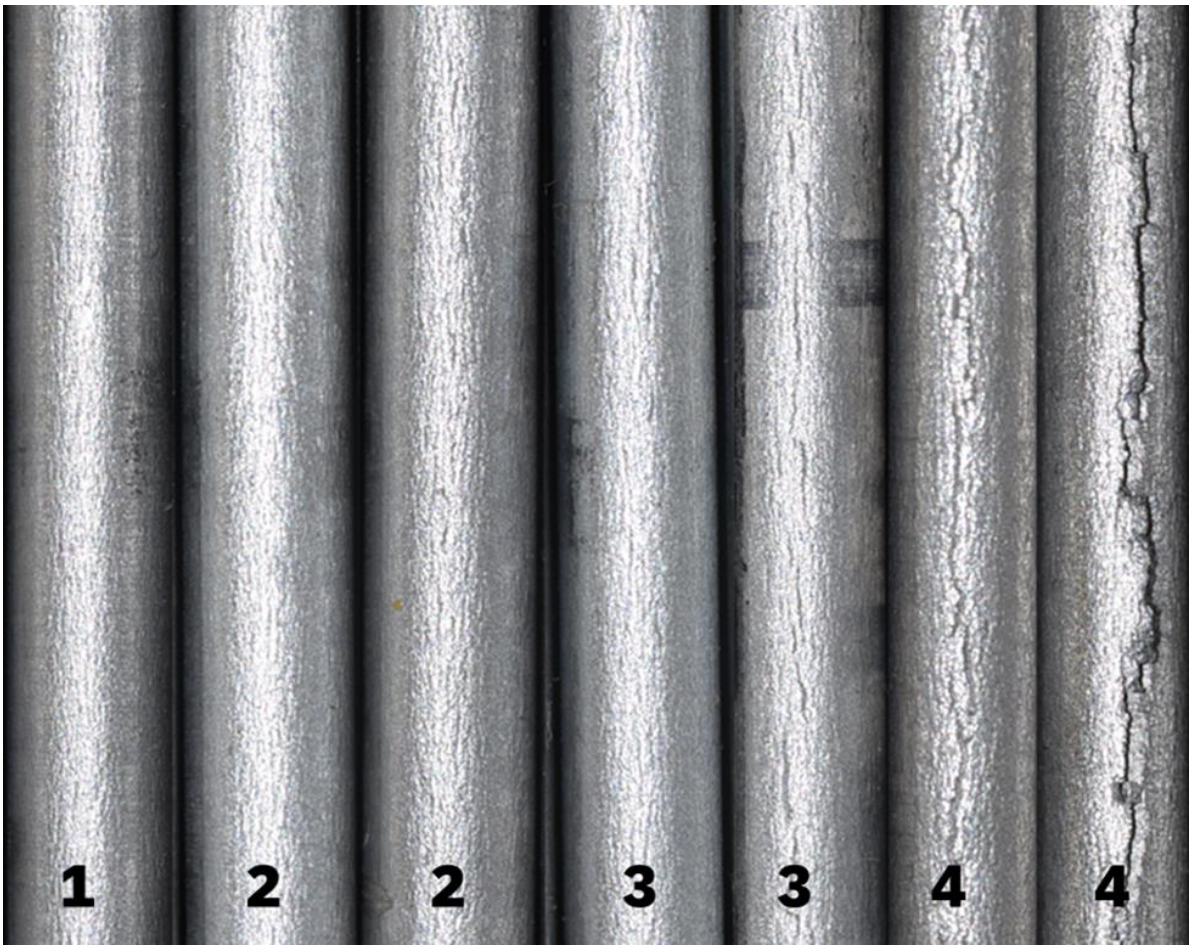

Figure 8: Ford Flat Hem Rating Scale from 1 to 4 per Ford BB 115-01

Figure 8 demonstrates the subjectivity and range of appearances for a given hem rating. Each rating can be considered a bucket in which a range of appearances may be fall. For example, three samples in **Figure 8** are given a rating of “3” but can be further discretized based on the proximity to adjacent ratings. The rightmost sample rated as a “3” in **Figure 3** may be

characterized as a “3+”, as the sample is almost, but not quite worthy of a “4”, while the leftmost “3”-rated sample in **Figure** 8 may be a “3-” as the sample is close to a “2” but does exhibit faint lines that typically are indicative of crack initiation. For the purposes of this study, a more discretized rating scheme based on the Ford scale was used to better account for this subjectivity and is provided in **Table 8**. Note that, in practice, a hem rating of 1 is extremely rare for aluminum alloys; such a rating might only be achieved for material with exceptional hem performance with a natural age near zero days.

Table 8: Detailed Rating Scale of Hem Performance with Assigned Numerical Values

Ford Rating	Ford Description	Detailed Rating	Description	Numeric Value
1	No Orange Peel	1	No Orange Peel	1
2	Mild to Heavy Orange Peel	2-	Fine Orange Peel	2.25
		2	Moderate Orange Peel	2.5
		2+	Coarse Orange Peel	2.75
3	Crack Initiation lines	3-	1-2 Faint Crack Initiation Lines	3.25
		3	Crack Initiation Line Across Width of Sample	3.5
		3+	Nearly Continuous Faint Cracks	3.75
4	Continuous cracks or through-thickness failure	4-	Large, Non-Continuous Cracks or Continuous, Faint Cracks	4.25
		4	Large, Continuous Cracks	4.5
		4+	Through Thickness Failure	4.75

Given the subjective and qualitative nature of the data generated by the Ford flat hem test, the VDA bend test was used to quantitatively assess formability and, by proxy, hem performance. This three-point bend experiment is commonly employed by European OEMs and similar to the Ford flat hem test, utilizes a combination of tensile pre-strain and bending to assess the local

formability via measurement of the bend angle at peak load. Prior to bending, samples are sheared into 300 mm x 70 mm coupons (longitudinal and transverse to the rolling direction) and strained 10% along the 300 mm axis. Two 60 mm x 60 mm specimens are then machined from each coupon, with four duplicate specimens tested per condition. During the experiment, the sample is supported by two rollers with a set gap of 2.54 mm. A punch with a radius of 0.2 mm is used to apply force to the center of the sample, causing the sample to bend [22]. The load is measured while the punch extends, with extension stopped just after peak load. The bend angle is then measured/calculated, yielding the key parameter reported by the test. A diagram of the experimental setup is shown below in **Figure 9**.

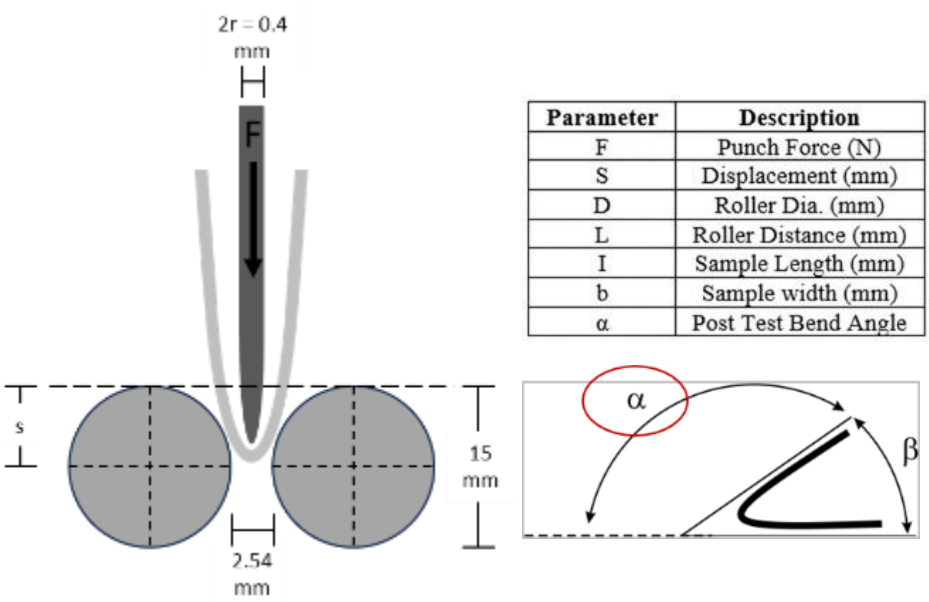

Parameter	Description
F	Punch Force (N)
S	Displacement (mm)
D	Roller Dia. (mm)
L	Roller Distance (mm)
I	Sample Length (mm)
b	Sample width (mm)
α	Post Test Bend Angle

Figure 9: Schematic of VDA Bend Test Performed on 6XX0, 6XX1, and 6XX2 Sample

2.5 Microscopy and Characterization

Optical microscopy was used as the primary tool to view general microstructural characteristics of as-cast, F-temper, and T-temper samples. In each case, samples were prepared by cutting into small pieces so that three samples can be mounted in each metallography "puck," a 5 cm diameter polymer cylinder that is employed to hold samples in place during preparation and follow-on microscopy. As-cast samples were viewed in the L-ST plane, while F-temper and T-temper samples were viewed in the L-LT (t/2; half-thickness location), L-ST, and LT-ST planes. After mounting, the samples were ground and polished using incrementally finer grits of SiC grinding paper, eventually finishing with a silk cloth and 1-micron diamond spray. At this point, images were taken to document the as-polished condition. **Figure 10** shows a T-temper sample of 6XX0-80% CW (P0080; **Table 8**) in the as-polished condition (top). In this condition, constituent and precipitate phases are clearly visible with little to no visibility of grain boundaries. To increase contrast and slightly accentuate grain boundaries, as-cast samples were also viewed after etching. Etching was performed by immersing samples in a mixture of 33% water, 33% HNO_3, 33% HCl, and 1% HF (by volume) for 30 seconds followed by immediate rinsing and drying. An image of the same 6XX0-80% CW sample (P0080; **Table 8**) is shown in **Figure 10** (bottom).

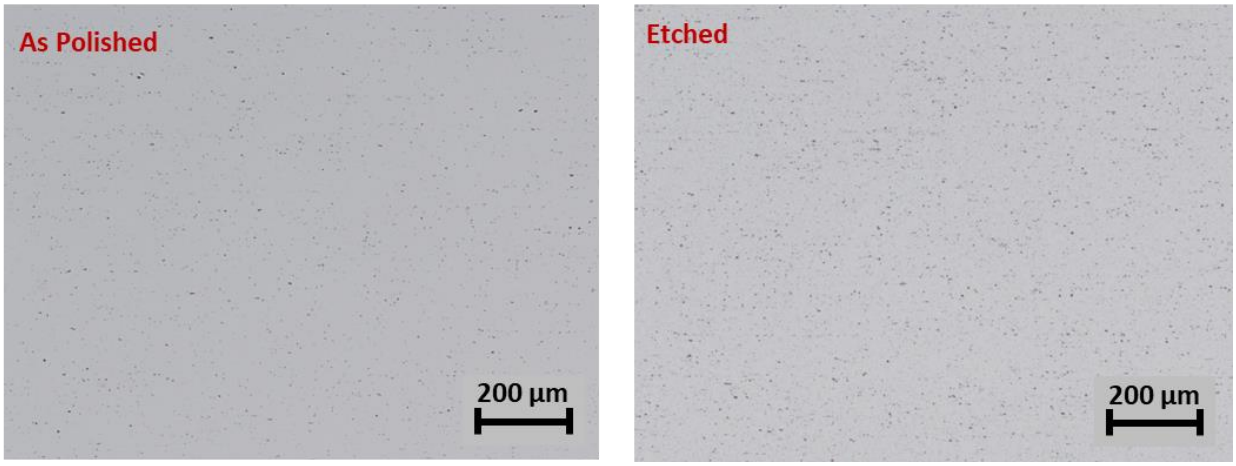

Figure 10: 100X Optical Micrograph of L-ST Plane of 6XX0-T4, 80% CW in As-Polished Condition (left) and Etched Condition (right)

Samples were also viewed after anodization to observe the grain structure of the samples more clearly. This process utilizes a 3% solution of fluoroboric acid (HBF_4) in water and a Buehler Electromet 4 to electropolish and anodize the samples. When viewed in the microscope, each grain will appear to be a slightly different color due to the differing orientations of the grains. **Figure 11** shows how the grain structure of the same T-temper 6XX0-80% CW (P0080; **Table 8**) is clearly observed after this electropolishing step.

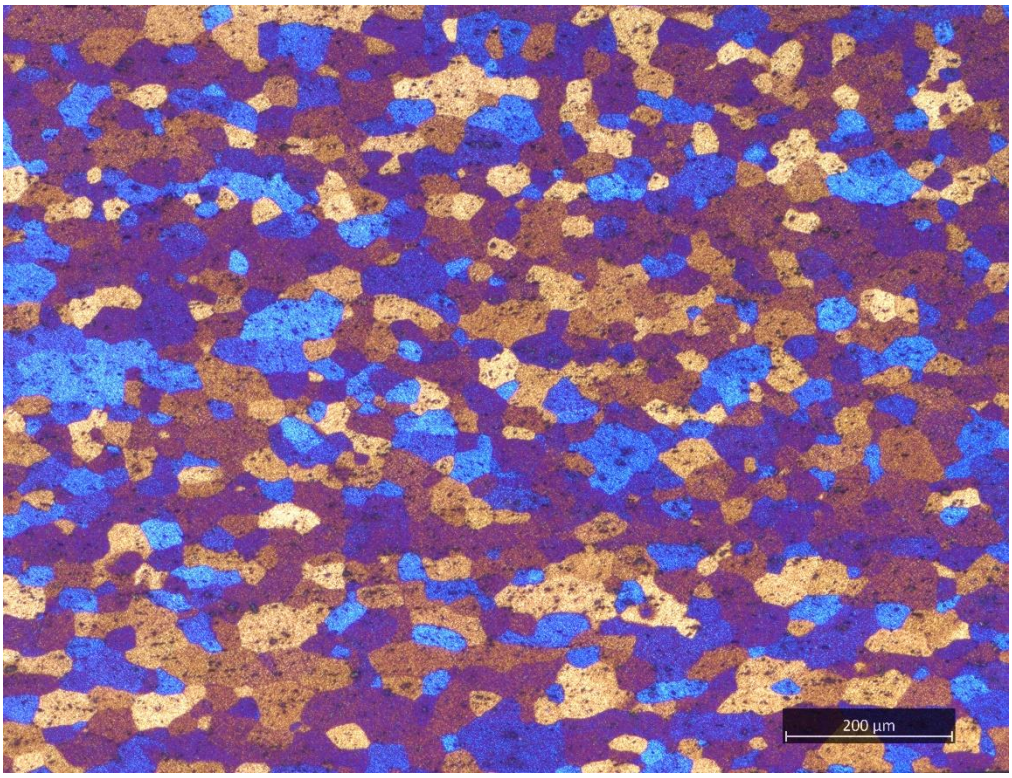

Figure 11: 100X Optical Micrograph of L-ST Plane of 6XX0-T4, 80% CW in Electropolished and Anodized Condition

Scanning electron microscopy was used for quantification of Mg_2Si and Al-Fe-Si constituent particles. Samples were prepared in a similar manner to the optical metallography samples and viewed in the as-polished condition only. The procedure for quantifying these phases was completed according to ASTM E1245-03. This method uses proprietary software to identify, count, and measure the area of both precipitate and constituent phases across a grid of images of a given sample. A grid of 65 images, taken at 1000x magnification, was used for phase quantification of all samples. Images were taken with negative 75% overlap to ensure particle were not double counted by the software. The software then outputs various metrics including total number of particles, number weighted average particle size, area weighted average particle size, and area %

of particles. In the SEM images, Mg_2Si generally appear black or significantly darker than the matrix, while constituent phases are white; an example of typical constituent phase morphologies and contrast are shown in **Figure 12**, with Mg_2Si and constituent phase particles identified by the red arrows.

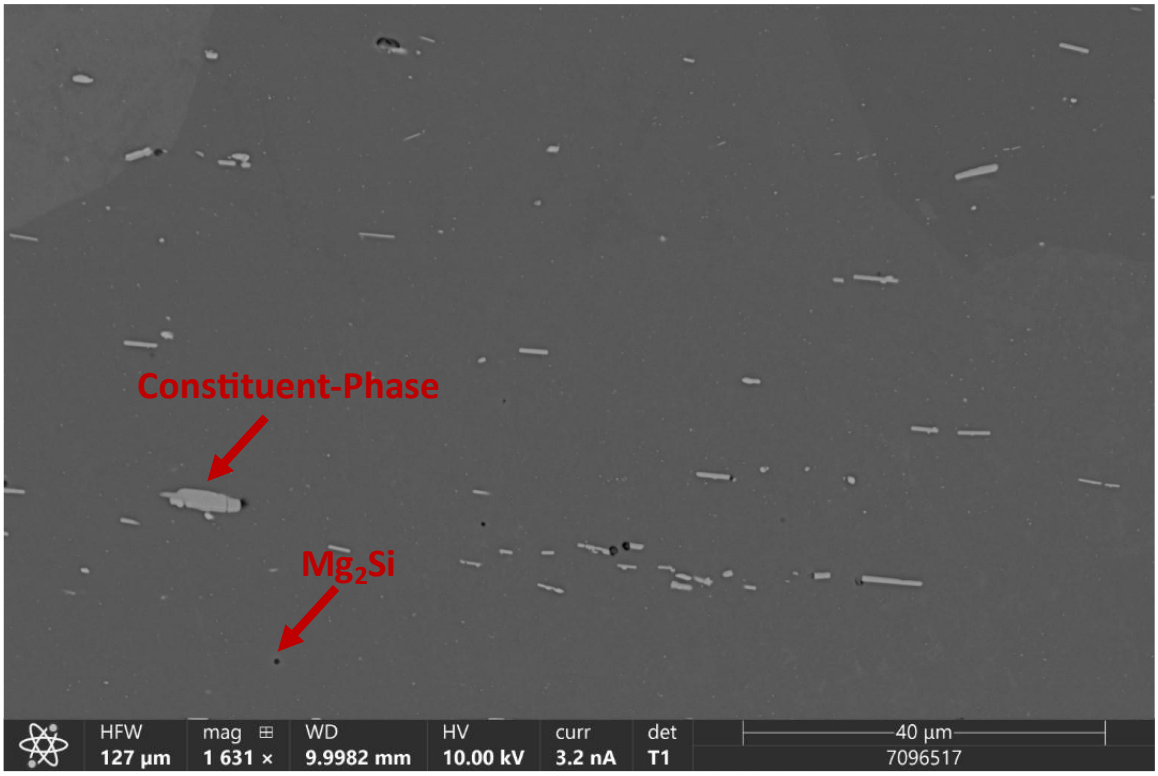

Figure 12: 1000X Electron Micrograph of L-ST Plane of 6XX0-T4, 70% CW

Finally, electron backscatter diffraction (EBSD) was used to evaluate grain morphology and texture as well as measure grain size. EBSD results were evaluated using proprietary analysis scripts, which provide the number-weighted and area-weighted average grain size and grain size distributions, grain boundary character distribution, pole figures, and fraction of grains with

specific texture components (e.g., cube, Goss, etc.). An example of a typical inverse pole figure (IPF) map, with associated IPF legend, for the alloys in this study is shown in **Figure 13**.

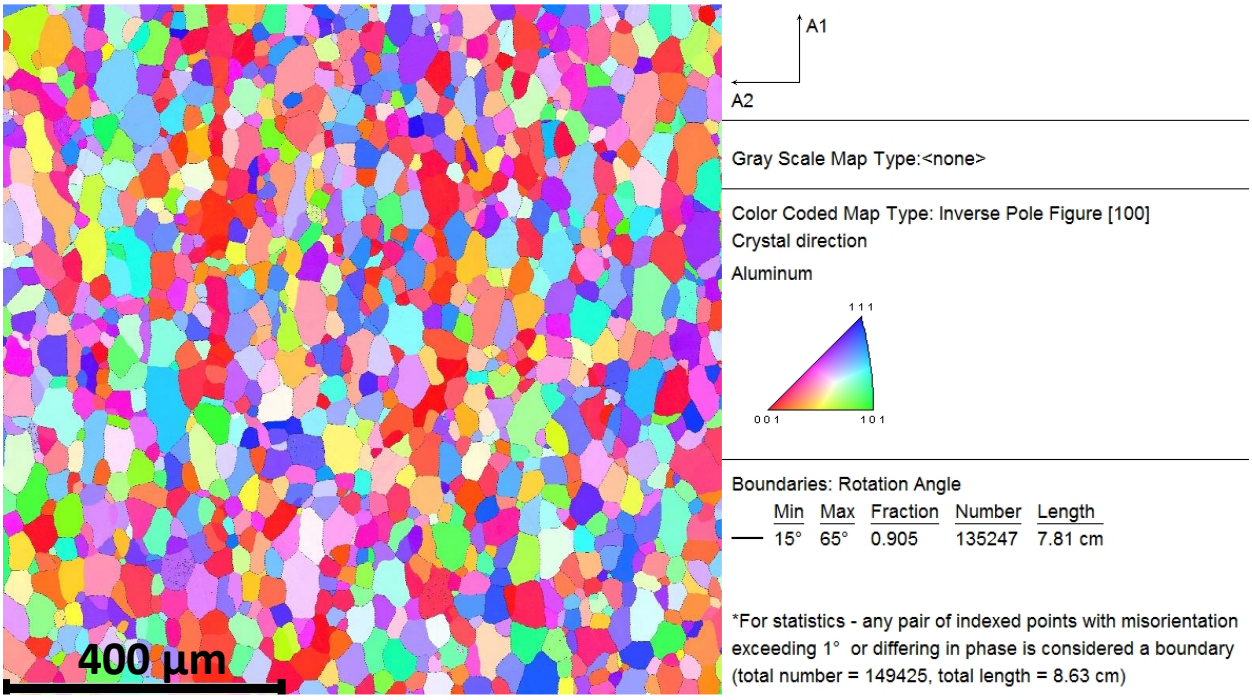

Figure 13: Representative inverse pole figure map of 6XX0-T4, 80% CW

3.0 Results

3.1 Microscopy and Characterization

Characterization of each of the three alloys began with optical metallography of as-cast samples to determine if the differences in chemistry led to noticeable differences in grain structure and secondary phase distribution in the as-cast condition. For this evaluation, samples were taken from the center thickness, quarter width location of the ingot so that the microstructure was representative of the ingot bulk. Representative micrographs are shown below in **Figure 14**. Qualitative examination suggests that notable differences do exist between the alloy compositions. For example, the 0% scrap alloy, 6XX0, exhibits noticeable larger grains and narrower grain boundaries relative to the scrap-bearing alloys. Conversely, differences between the 33% and 67% scrap (6XX1 and 6XX2) alloys are more subtle, though 6XX2 appears to have slightly finer grains and narrower grain boundaries. The composition of the grain boundaries is made up of elements which form a eutectic with aluminum, including Mg, Si, Cu, and Fe.

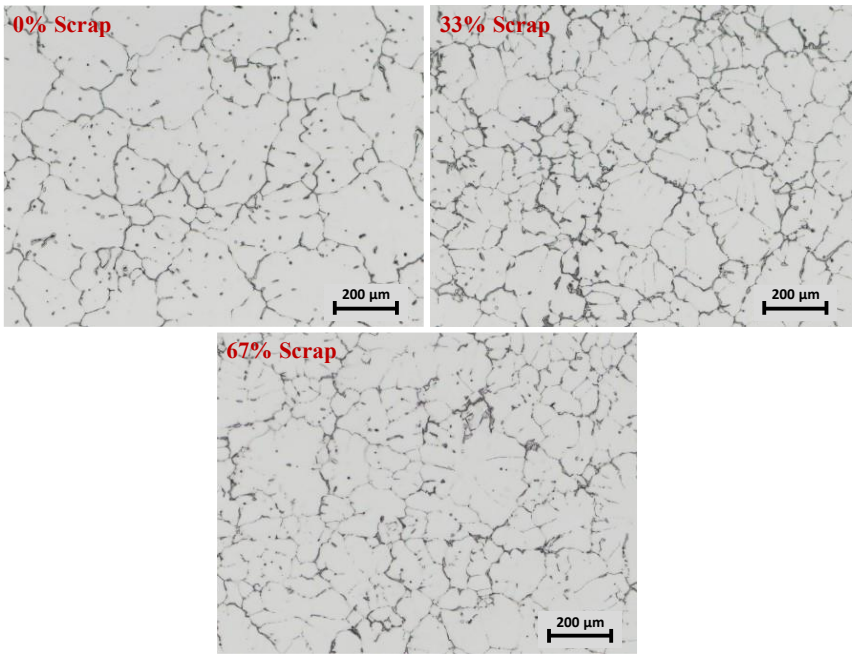

Figure 14: 100X Optical Micrographs of As-Cast Samples of 6XX0, 6XX1, and 6XX2 in Etched Condition

Similarly, F-temper samples were viewed in the as-polished condition, to survey the levels of Mg_2Si and constituent phases before heat treatment. Because some of the alloys have a substantial amount of constituent phase, it can be easy to misidentify particles in F-temper samples. When viewing in the as-polished condition, Mg_2Si will appear darker than constituent phases and have a blueish tint or halo. As shown in **Figure 15**, examination of the various alloys indicates that none have an especially clean microstructure. In fact, the Mg_2Si content appears to be similar across the tested conditions, with each sample displaying a mixture of finer (< 1 µm in diameter) and coarse (1-3 µm in diameter) particles.

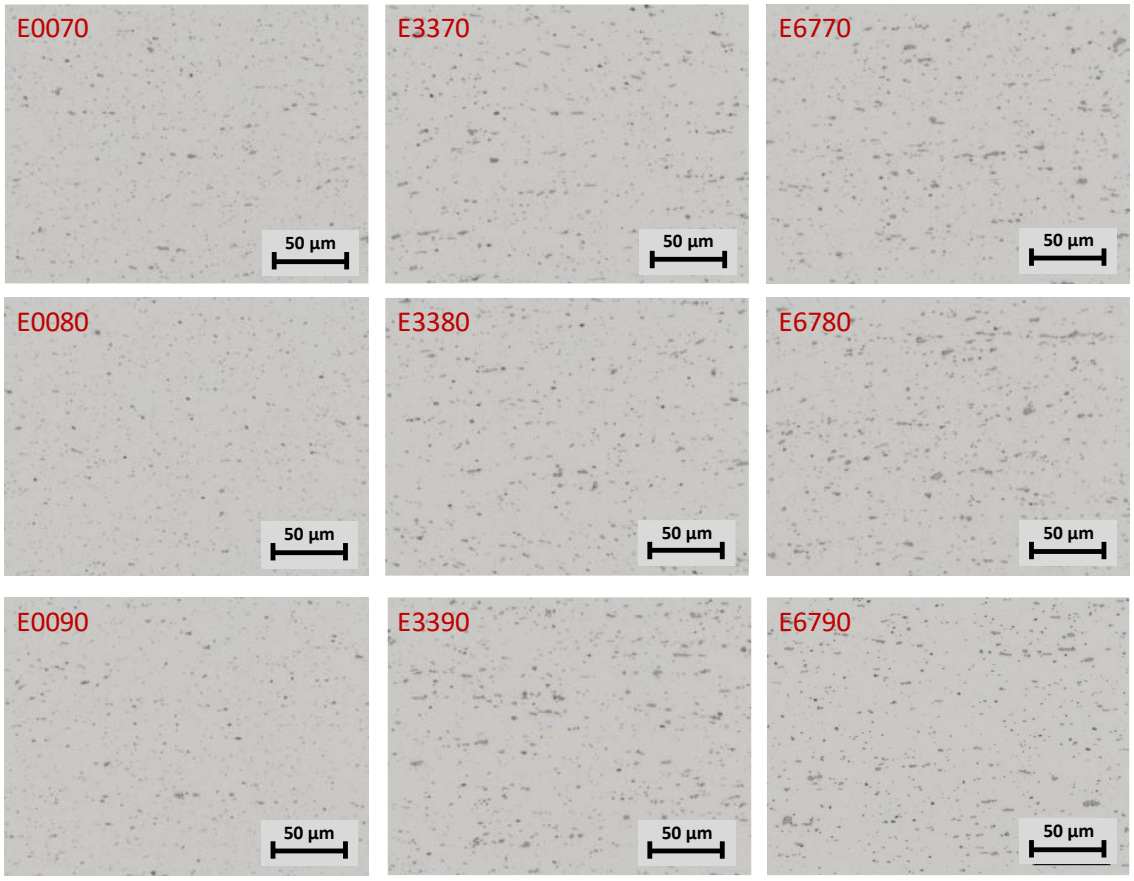

Figure 15: 500X L-ST images at T/2 of F-temper Samples in As-Polished Condition. Scale Bars Indicate 50 µm.

All equivalent strength, T-temper samples were viewed in the as-polished condition for a general survey of constituent and precipitate appearance; **Figure 16** provides example micrographs for each condition taken at the mid-thickness (t/2) of the sheet in the L-ST plane at 500X magnification. Course Mg_2Si particles, indicated by the black particles with a blueish tint, are visible in all conditions, with the number of particles appearing to decrease with increasing recycle content. As expected, the cold work percentage does not seem to have a consistent impact on the number of particles; such results may be due to unintentional variations in processing characteristics during high temperature treatment of each sample. Additionally, the amount of

Al_9Fe_2Si and $Al_{12}(Fe,Mn)_3Si$ constituent, which appear as darker grey particles, significantly increases as recycle content increases. The increasing amount of this phase likely accounts for the decrease in Mg_2Si observed in the higher scrap utilization alloys.

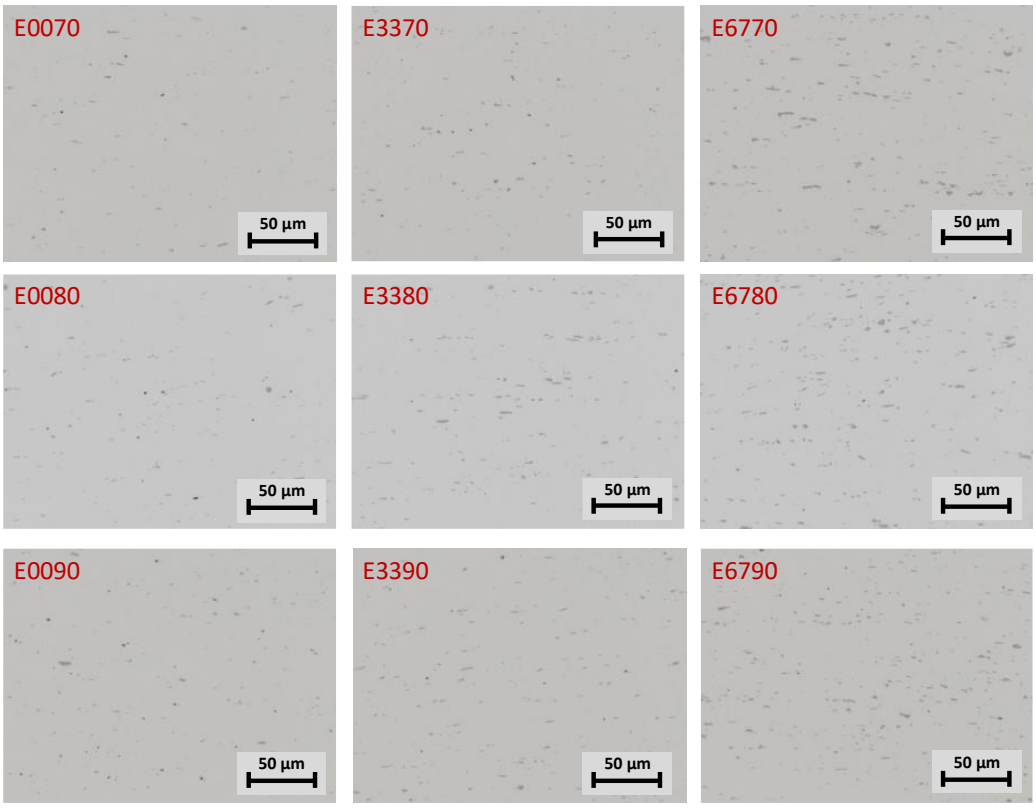

Figure 16: 500X L-ST Images at T/2 in As-Polished Condition of Equivalent Strength Samples. Scale bars indicate 50 microns. Contrast increased 25% to improve particle visibility.

To confirm the visual observations of the as-polished samples, the distribution and morphology of the Mg_2Si and constituent particles were quantified using scanning electron microscopy. A total area of approximately 700,000 μm^2 across 63 images was measured for quantification of phases. Due to material and resource constraints, only the 70% and 90% cold work version of the equivalent strength condition for each alloy were selected for analysis. However, this truncated matrix will still provide representative insights given that main influences on Mg_2Si characteristics are expected to be cooling profiles during hot rolling and solution heat

treatment. **Table 9** summarizes the particle area % and number-weighted average size determined from this analysis. Contrary to initial visual observations from **Figure 16**, Mg_2Si levels were observed to be much higher in the 90% cold reduction condition relative to the 70% cold reduction version of each alloy composition. Interestingly, these electron microscopy results indicate that the Mg_2Si particles in the 90% cold reduction samples were slightly coarser and much more numerous than in 70% CW samples, with a 2 to 5 times higher area percentage of Mg_2Si observed in the higher cold reduction lots. This result can potentially be explained by variations in the cooling rates during the hot working of each condition due to the differences in sheet gauge for the 70 and 90% cold work levels. Regardless, both 70% and 90% CW samples generally followed the expected trend of Mg_2Si slightly decreasing with increased scrap usage. Notably, the 90% cold work samples of 6XX2 did have slightly more Mg_2Si than other samples, though the coarser average particle size suggests these samples likely experienced slower than expected cooling rates during hot rolling.

Table 9: Mg_2Si Content of 70% and 90% Cold work, Equivalent Strength Samples of 6XX0, 6XX1, and 6XX2

Lot Number	Number Weighted Average Mg2Si Particle Equivalent Diameter (μm)	Area Weighted Average Mg2Si Particle Equivalent Diameter (μm)	Mg2Si Particle Equivalent Diameter Standard Deviation (μm)	Mg2Si Particle Area Fraction (%)
E0070	0.805	1.131	0.369	0.053%
E0090	0.778	1.226	0.403	0.136%
E3370	0.722	1.063	0.358	0.036%
E3390	0.810	1.215	0.397	0.112%
E6770	0.763	1.040	0.336	0.026%
E6790	0.845	1.189	0.380	0.142%

The amount of constituent phase, which predominantly forms and is therefore set during ingot solidification, more closely adhered to expected trends. As shown in **Table 10**, the

constituent phase area percentage increased directly with scrap utilization level but did not vary significantly with cold work percentage. However, the constituent particle size was found to be slightly coarser as the area fraction increased and it appears that higher cold work has perhaps a slight impact on reducing particle size. For example, the average particle size was approximately 10% lower for the 90% cold work samples of 6XX0 and 6XX1 than was observed in the 70% cold work condition. However, this trend did not hold for 6XX2, which only exhibited a 3% particle size increase in higher cold work samples relative to the lower cold work condition.

Table 10: Constituent Particle Content of 70% and 90% Cold Work, Equivalent Strength Samples of 6XX0, 6XX1, and 6XX2

Lot Number	Number Weighted Average Constituent Particle Equivalent Diameter (μm)	Area Weighted Average Constituent Particle Equivalent Diameter (μm)	Constituent Particle Equivalent Diameter Standard Deviation (μm)	Constituent Particle Area Fraction (%)
E0070	0.879	1.511	0.489	0.375%
E0090	0.842	1.453	0.465	0.360%
E3370	0.984	1.760	0.577	0.920%
E3390	0.937	1.566	0.516	0.850%
E6770	1.057	1.845	0.614	1.127%
E6790	1.075	1.909	0.626	1.151%

All equivalent strength samples were also viewed in the anodized condition for comparison of the grain structure, shown in **Figure 17**. As expected, the 70% cold reduction samples exhibited the largest grain size for each alloy, with grain size generally decreasing with increasing cold work level. Interestingly, there a strong impact of increased recycle content on grain size, with the 33% and 67% scrap alloys having successively smaller average grain sizes. In

fact, the incorporation of 33% and 67% recycle content appears to be nearly as effective at reducing the grain size than the impact of an additional 10-20% cold work in the control alloy.

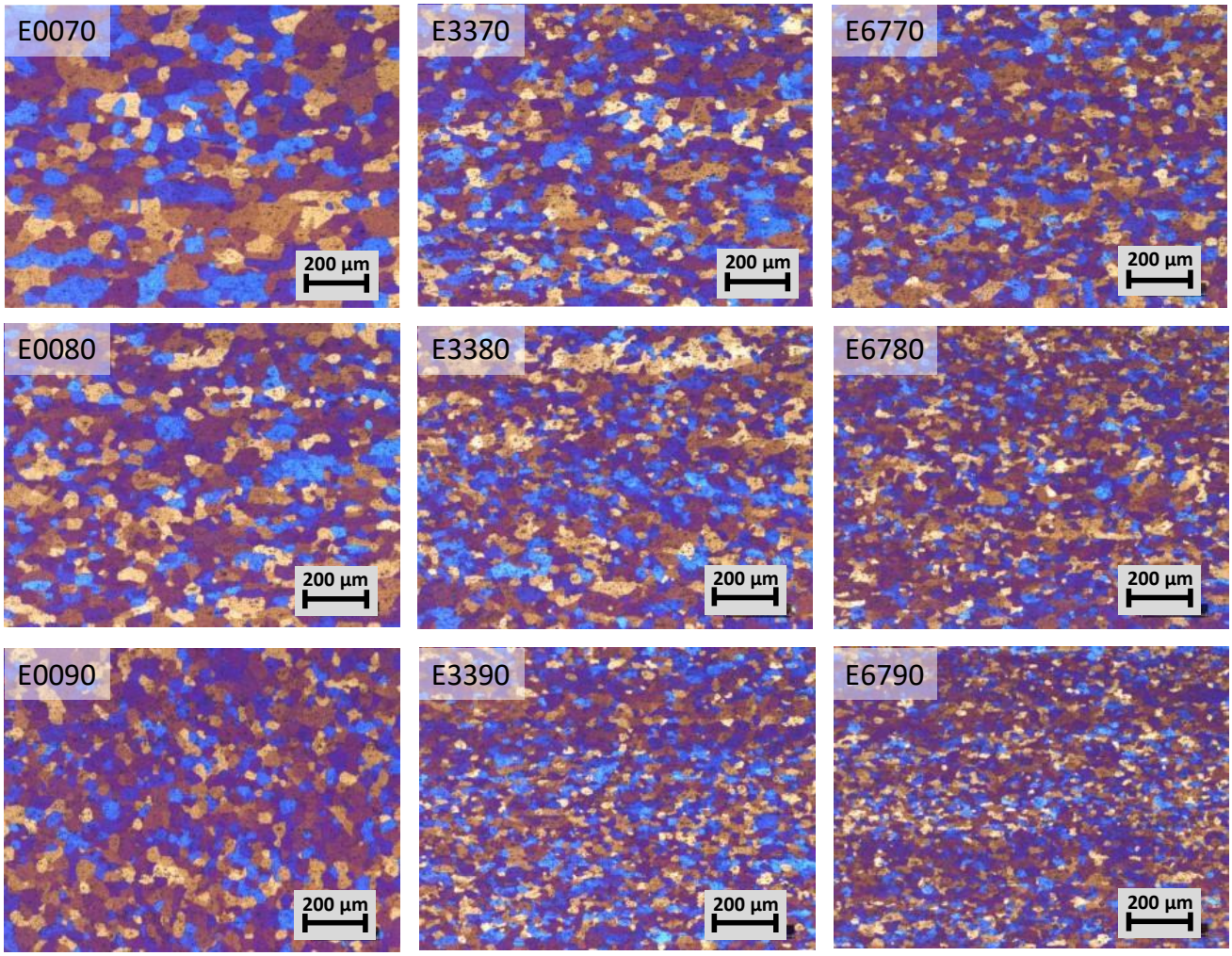

Figure 17: 100X L-ST Images at T/2 in Electro-polished and Anodized Condition of Equivalent Strength Samples. Scale bars indicate 200 µm.

EBSD was used to quantify the grain size for each lot; the average grain size for each condition, based off a scan height and width of approximately 1000 microns, is reported in **Figure 18**. The results of this grain size analysis largely confirm the initial observations from the anodized images in **Figure 17**. These data demonstrate that the impact of the grain refinement effects from increasing scrap does not linearly scale with the fraction of recycled content. For example, the

number-weighted grain size for the 33% scrap alloy is 30 to 40 % smaller than the control alloy, while the number-weighted grain size of the 67% scrap alloy is ~10 % smaller than the 33% scrap alloy. Referring to **Table 9** and **Table 10**, this could be explained by the increase in average Al-Fe-Si constituent particle size from the increasing iron and manganese content as scrap content increases. Specifically, the increase in particle size limits the number of particles that can act as grain nucleation sites, which thereby limits the grain-refining impacts of the constituent phases. Additionally, though the effect of the coarse Mg_2Si particles on particle-stimulated nucleation is likely small, the observed decrease in this phase with increasing recycled content would also act to lower the extent of reduction in grain size with additional scrap.

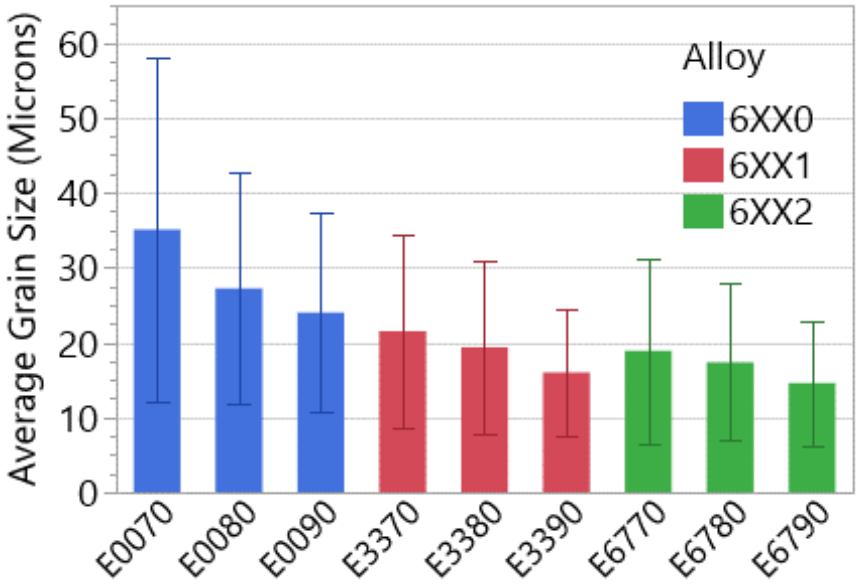

Figure 18: Number-Weighted Average Grain Size of "Equivalent Strength" Lots as measured by Electron Backscatter Diffraction. Error Bars Reflect Number Weighted Grain Size Standard Deviation

3.2 Tensile Testing

As discussed in Section 2, uniaxial tensile experiments were performed on each condition on a monthly basis through 6 months of natural aging. These experiments were performed to ensure that each lot was adhering to Ford specification requirements as well as provide context for the subsequent bend performance evaluations. Natural aging curves for each of the "equivalent strength lots are shown in **Figure 19**; note that both individual data points and a data smoothing line. Despite efforts to normalize each specimen for strength during the modeling performed in Section 2, results demonstrate that samples within a given condition exhibited variations of ~10 MPa in yield strength at each aging interval, with strength decreasing with increasing scrap utilization and increasing cold work. These results suggest that the regression model used to develop the heat treatment practices likely underestimated the impact of alloy composition and overestimated the impact of cold work on the alloy yield strength. Regardless, all lots appeared to naturally age at similar rates despite the differences in alloy composition and reside well within Ford WSS-A174-A2 yield strength limits (dashed lines in **Figure 19**). For all lots, the yield strength was higher when measured in the longitudinal direction than strength measured transverse to the rolling direction, though the observed difference was typically less than 5 MPa. While all alloys were within the governing specification, it does appear that the control alloy composition conditions (E00XX) did have more variability than both corresponding scrap alloy conditions (E33XX and E67XX, respectively). This is likely due to the control alloy composition targeting a higher level of undissolved Mg_2Si during solution heat treatment, resulting in an increased sensitivity to any variability in the laboratory-scale heat treatment. Examples of such inherent variability include an observed +/- 5 second window in which samples were removed from heat

treatment furnaces and the subtle differences in the degree of sample warping during heat treatment.

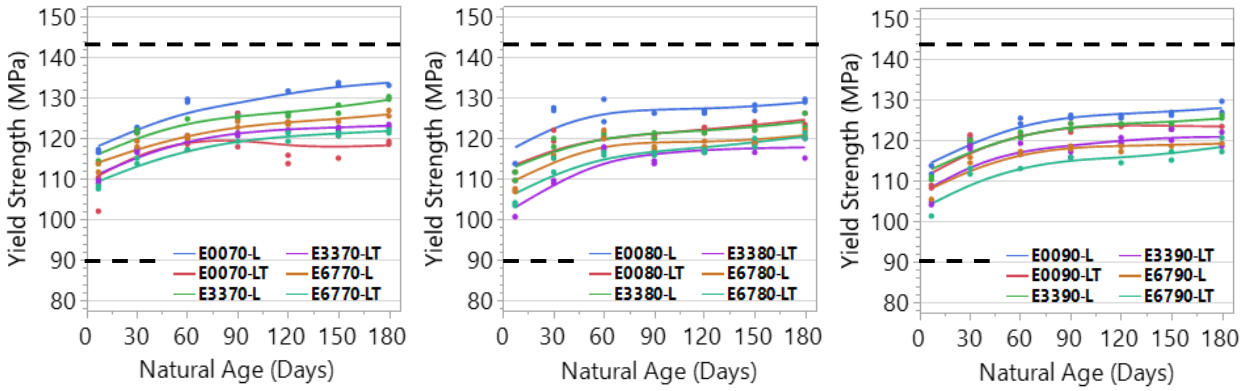

Figure 19: Yield Strength Natural Aging Curves of "Equivalent Strength" Lots in L and LT Directions. Ford Specification Limit Indicated by the Dashed Lines.

While the variability in measured yield strength was notable for the “equivalent strength” conditions, the “peak strength” lots exhibited more consistent behavior, as demonstrated by the natural aging curves shown in **Figure 20**. This reduction in variability arises from the fact that these samples targeted full dissolution of Mg_2Si, which resulted in a reduced sensitivity to small, unintentional variations in heat treatment duration. All “peak strength” conditions demonstrated an increase in yield strength relative to the analogous “equivalent strength” conditions. Specifically, the control composition (P00XX) yield strength increasing by ~10 MPa, the 33% scrap alloys (P33XX) yield strength increasing by ~5 MPa, and the 67% scrap alloys (P67XX) increasing in strength by 1 to 3 MPa relative to the associated EXXX specimens. Comparison of the strength trends reveals that increasing scrap utilization typically lowered strength for a given cold work level, while increasing the cold work level for a constant scrap utilization led to higher strengths. Additionally, as with the “equivalent strength” lots, the yield strength was found to be

higher for specimens tested with the tensile axis parallel to the rolling direction versus transverse to the rolling direction. Finally, all samples meet the yield strength requirements from the governing Ford specification; however, the control composition (P00XX) conditions to appear to be nearing the maximum limit by 180 days of natural aging.

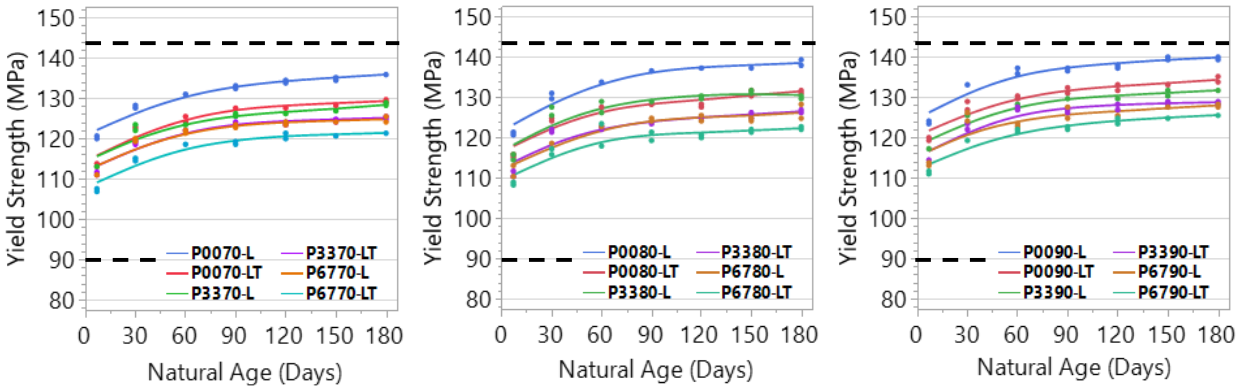

Figure 20: Yield Strength Natural Aging Curves of "Peak Strength" Lots in L and LT Directions. Ford Specification Limit Indicated by the Dashed Lines.

The evolution of the ultimate tensile strength largely follows the same trends as yield strength for each grouping of alloys, as shown in **Figure 21** and **Figure 22** for the “equivalent strength” and “peak strength” conditions, respectively. In general, the ultimate tensile strength decreases with increasing scrap usage for a given cold work level but increases with increasing cold work for a given scrap level. Overall, the differences in ultimate tensile strength between lots are similar to the differences observed for yield strength in **Figure 19** and **Figure 20**, though the ultimate tensile strength results have slightly less variability. This is likely due to the reduced impact of plastic strain, as may occur from warping during heat treatment, on ultimate tensile strength. Finally, all lots were found to meet the ultimate tensile strength requirements in the Ford specification for natural aging between 20 and 180 days. However, the peak strength lots of the control alloy composition with 80-90 % cold work (P0080 and P0090, respectively) began to

approach the Ford specification upper limit. As such, it is likely that these conditions may have issues meeting the specification limit in production and would likely need to target slightly lower levels of Mg and Si to reliably meet specification.

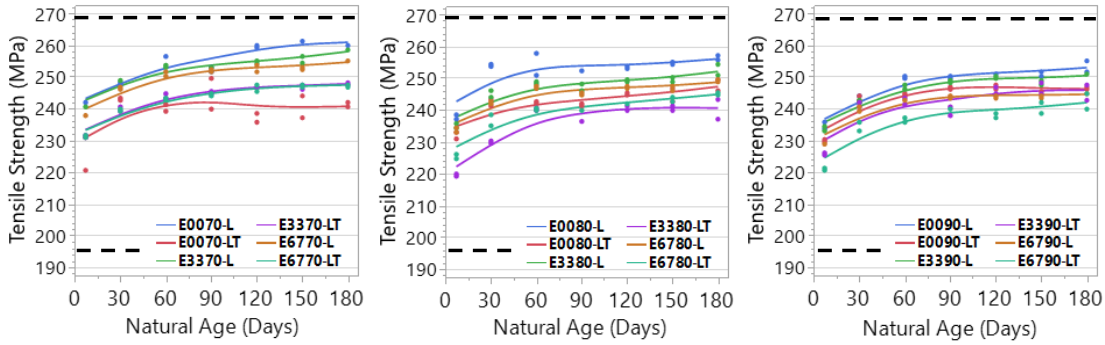

Figure 21: Tensile Strength Natural Aging Curves of "Equivalent Strength" Lots in L and LT Directions. Ford Specification Limit Marked by Dashed Lines.

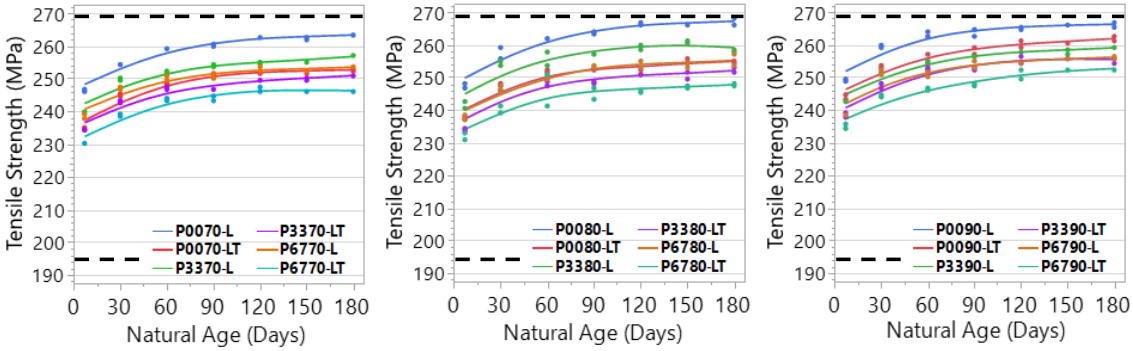

Figure 22: Tensile Strength Natural Aging Curves of "Peak Strength" Lots in L and LT Directions. Ford Specification Limit Marked by Dashed Lines.

Unlike yield and ultimate tensile strength, uniform elongation is not expected to significantly change as natural age increases. Therefore, data from all aging intervals were averaged for comparison as a method to decrease the impact of test variability on results; results as a function of composition and cold work level are shown in **Figure 23**. These data demonstrate that increases in recycle content and cold work generally decrease the uniform elongation; such

results are consistent with expectations for higher iron and manganese content alloys. However, it is interesting to note that while the control composition had reasonable similarity between the transverse versus longitudinal experiments, the transverse direction had distinctly lower elongation for the scrap alloys. Additionally, comparison of the equivalent and peak strength lots revealed similar uniform elongation, with peak strength conditions showing an improvement of 0 to 0.5% versus analogous equivalent strength material. Lastly, all samples meet the Ford specification minimums; however, 80% and 90% cold work samples of the 67% scrap alloy do approach the minimum allowable uniform elongation.

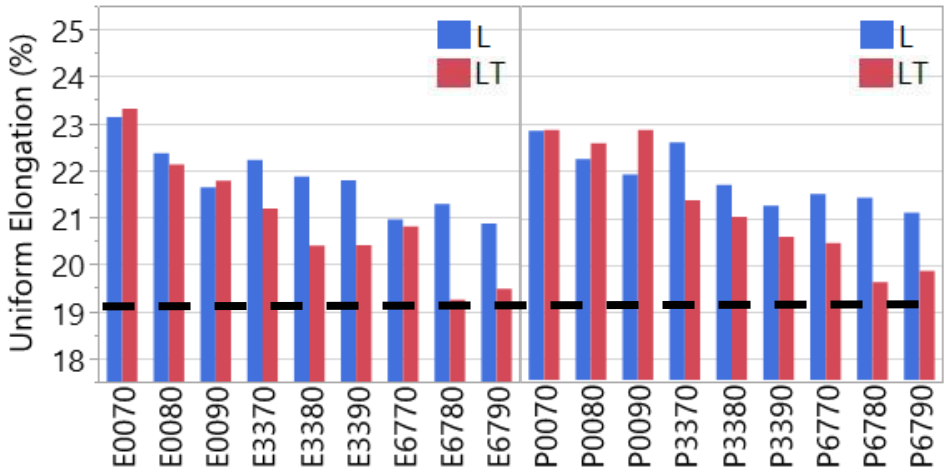

Figure 23: Average Uniform Elong. by Lot and Direction. Ford Spec. Marked by Dashed Line.

Though the Ford specification does not have a requirement for total elongation, it is still important to consider as factor in alloy formability; results as a function of composition and cold work level are shown in **Figure 24**. As with the uniform elongation, total elongation decreases with cold reduction and increasing alloy content. Similarly, the limited differences between the equivalent and peak strength conditions for a given composition-cold work combination were also observed. However, one notable difference was that the effect of directionality appeared to be even

more potent for total elongation than was observed for the uniform elongation. For example, manufacturers will commonly target between 22% and 24% for total elongation minimums, but essentially all lots with increased recycle content would fail to meet this criterion for the transverse direction.

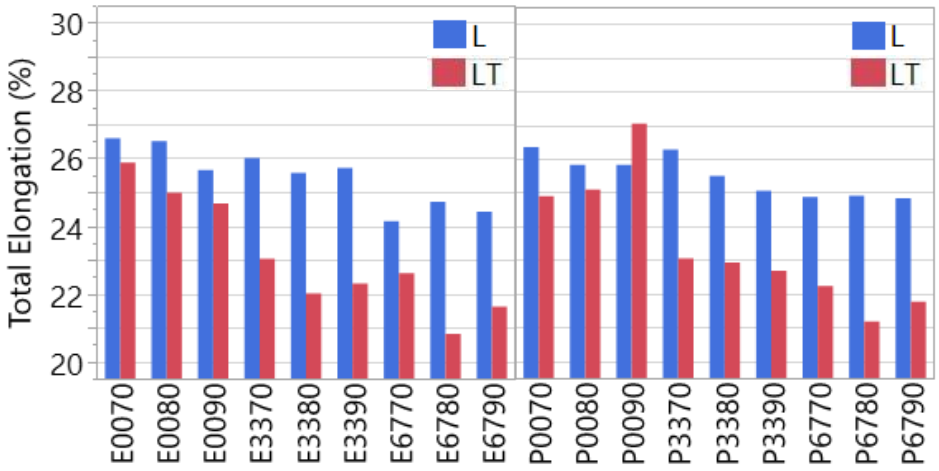

Figure 24: Average Total Elongation by Lot and Direction.

Plastic strain ratio, or r-value, is the ratio of the reduction of sample width to sample thickness during plastic deformation and is typically measured at 10% elongation per Ford specification requirements. Like elongation, this material property is not expected to significantly change with natural aging, and thus values across all testing intervals are averaged in **Figure 25**. These data reveal that additional scrap utilization results in a decrease in r-value for a constant cold work percentage, indicating increased thinning during deformation. Conversely, increased cold reduction generally increased the r-value for loading in the transverse direction, but had a more complex effect on the r-value of the longitudinal specimens, where 80% cold work appears to be consistently the best performer. Lastly, comparison of the “equivalent strength” and “peak

strength" alloys demonstrates that the P series conditions generally outperformed the analogous E series condition.

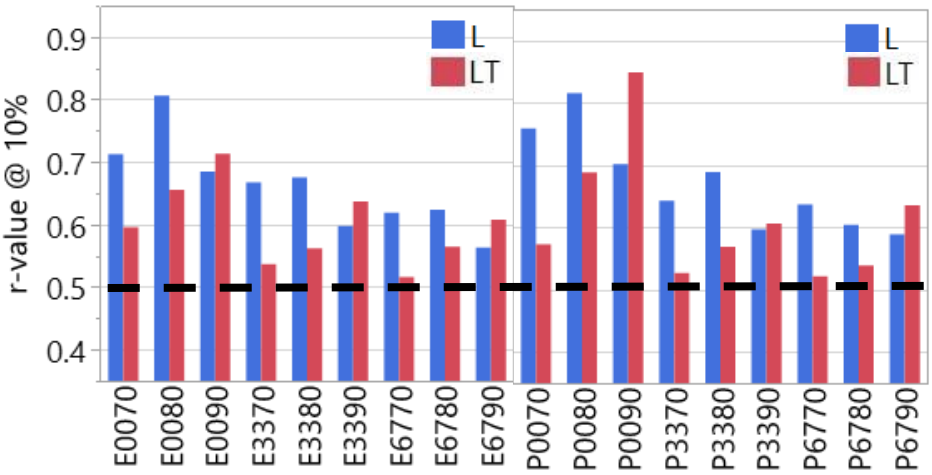

Figure 25: Average r-value (plastic strain ratio) @ 10% Elongation by Lot and Direction. Ford Specification Limit Marked by Dashed Line.

Finally, strain hardening exponent, or n-value, represents the slope of the stress-strain curve in the plastic deformation region. For the purposes of this study, this value was determined via a power-law to the stress-strain curve between 10-20% elongation, as is typically done in the automotive industry. Results for this analysis are shown in **Figure 26**. These data demonstrate that the strain hardening exponent generally decreases as the recycle content and level of cold work increases; this behavior was noted for both the "equivalent strength" and "peak strength" alloys, with limited differences between comparable conditions. Similarly, both alloys exhibited a higher n-value when uniaxially tested along the T-direction as compared to the L-direction for a constant composition-cold work combination.

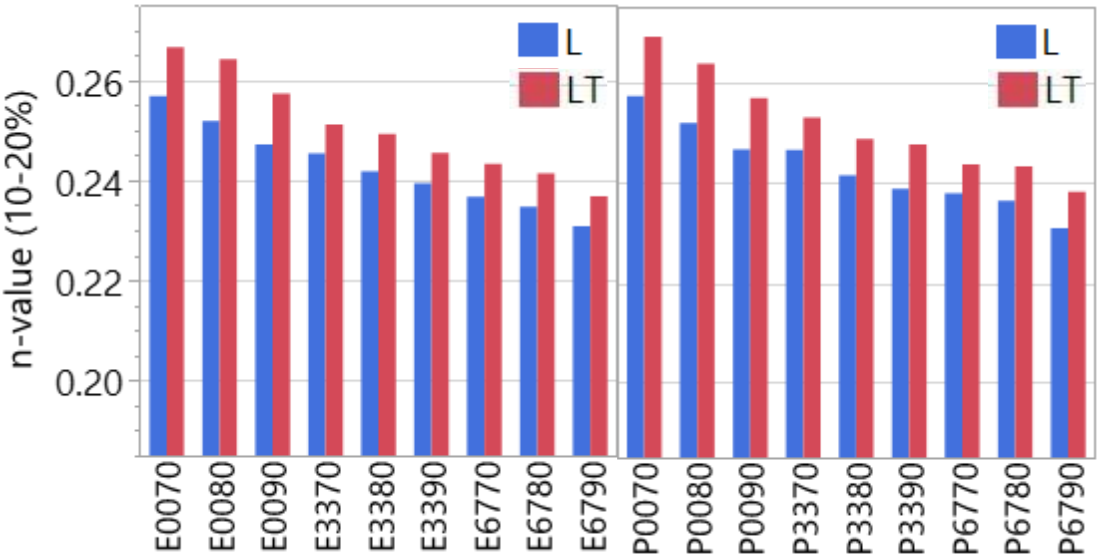

Figure 26: Average n-value (strain hardening exponent) from 10% to 20% Elongation by Lot and Direction. Ford Specification Limit Marked by Dashed Line.

3.3 Hem and VDA Bend Testing

As mentioned earlier, the hemming performance was evaluated for all conditions of interest at intervals of 30-, 90- and 180-days natural aging using the Ford flat hem method. The average hem ratings for each condition are summarized in **Figure 27**, with example images of the hems for the L-direction equivalent strength materials shown in **Figure 28**. Contrary to initial expectations, the control lots had by far the worst hem performance. Even at 30 days natural age, several conditions displayed crack initiation lines and thus, were given failing ratings. Surprisingly, both the moderate and heavy scrap usage alloys performed well when compared to the control lot. For example, the 80% and 90% cold work samples of the moderate scrap alloy

(P/E3380 and P/E3390), consistently performed better than other lots. Performance was generally similar in L and LT directions. A second notable observation is that the hem performance of each given lot with respect to natural aging time was slightly more variable than expected. In general, experience has demonstrated that as strength increases with natural aging, the hem performance of a given alloy will generally degrade. As such, the hem rating is expected to increase over time. One exception to this trend is that a material that performs particularly well at low natural aging times may have somewhat unchanging hem ratings over the course of its expected shelf life. This is seen in several of the higher cold work samples of P/E33XX and P/E67XX. Lastly, several examples are noted, particularly for the 70% cold work conditions, where the hem rating significantly increased between one and three months, but then dropped at six months. The root cause of this is likely variation in the thickness of samples, which is much more likely in lab processed materials than plant processed materials. The flat hem test is particularly sensitive to variations in gauge as the die sets the bend radius based on the nominal gauge of the material. Any departure from nominal gauge can result in a bend radius that is tighter than intended, resulting in poor hem performance.

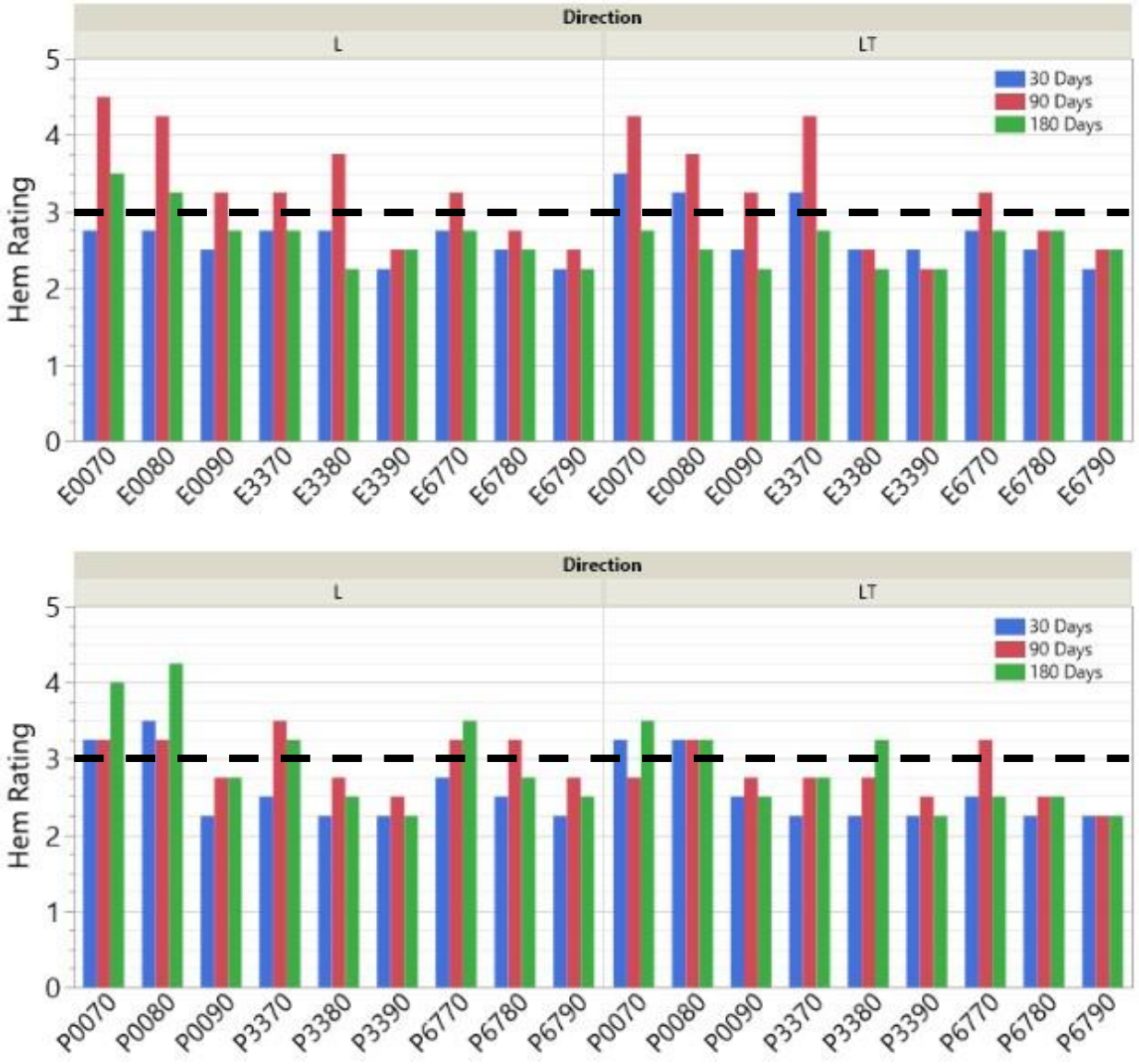

Figure 27: Flat Hem Simulation Results for each lot at 30 Days, 90 Days, and 180 Days Natural Age. Labeled Direction Indicated direction in which samples were cut. Ford Specification Limits marked by Dashed Line.

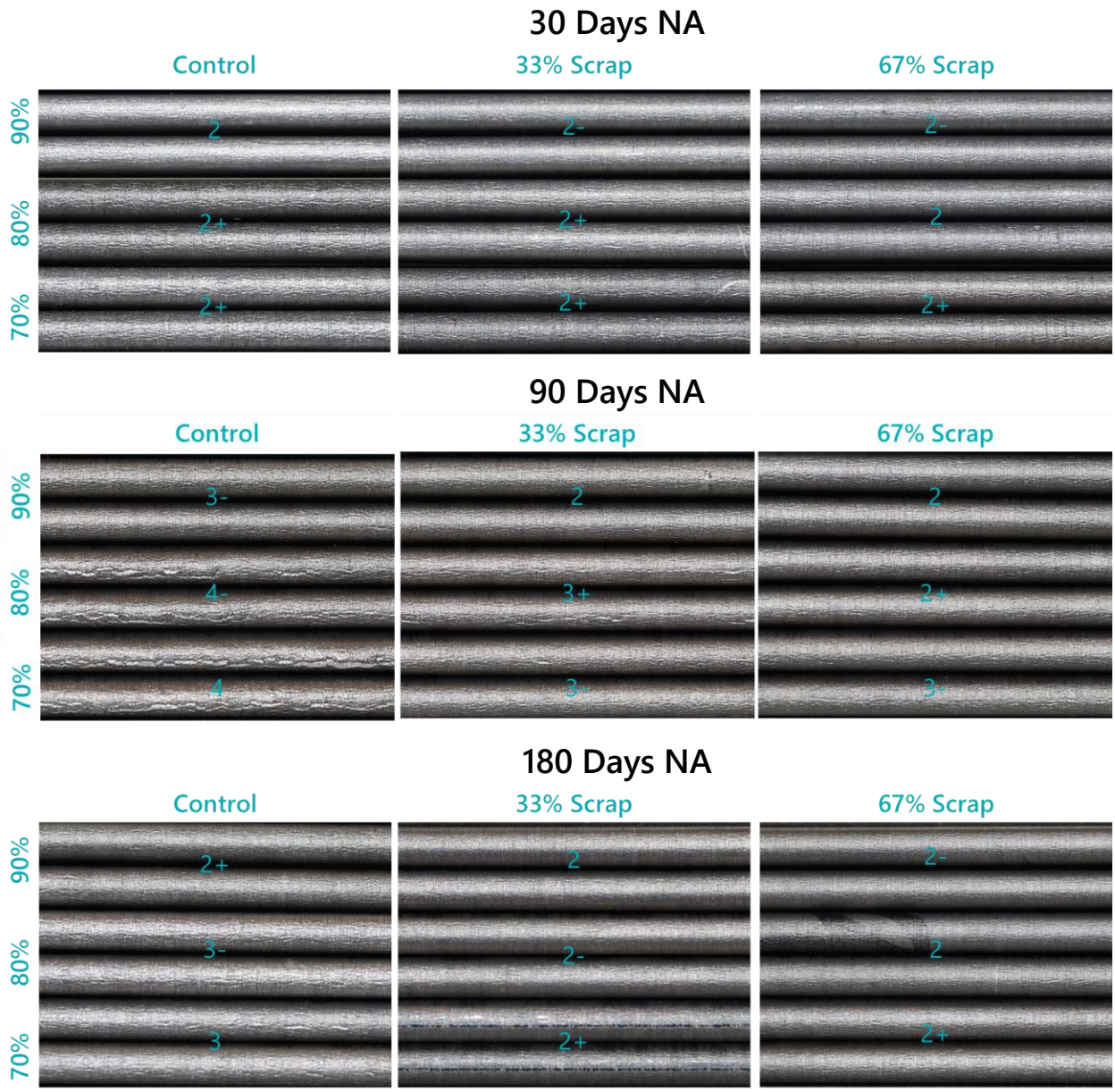

Figure 28: Flat Hem Simulation Sample Images of Equivalent Strength Lots, Tested at 30 Days, 90 Days, and 180 Days of Natural Age. Samples were cut in Longitudinal Direction.

The average bend angle determined from the more quantitative VDA bend experiments are shown in **Figure 29;** note that due to material constraints, only equivalent strength lots with 70% and 90% cold work were evaluated. One important difference between the VDA and hem

experiments is that higher values indicate improved performance for VDA testing since a larger bend angle reflects improved formability up to peak loading. Overall, the VDA bend testing revealed several notable insights. First, natural aging time appeared to have a stronger effect in degrading the bend angle of the 70% cold work condition relative to the 90% cold work condition for a given alloy when tested along the L direction. This behavior was less differentiated for testing along the LT direction. Second, increasing the cold work level generally improved the VDA bend angle obtained. Lastly, and most interesting, is that despite having generally poor performance during actual hemming experiments, the control composition specimens (E00XX) typically outperformed analogous higher scrap conditions.

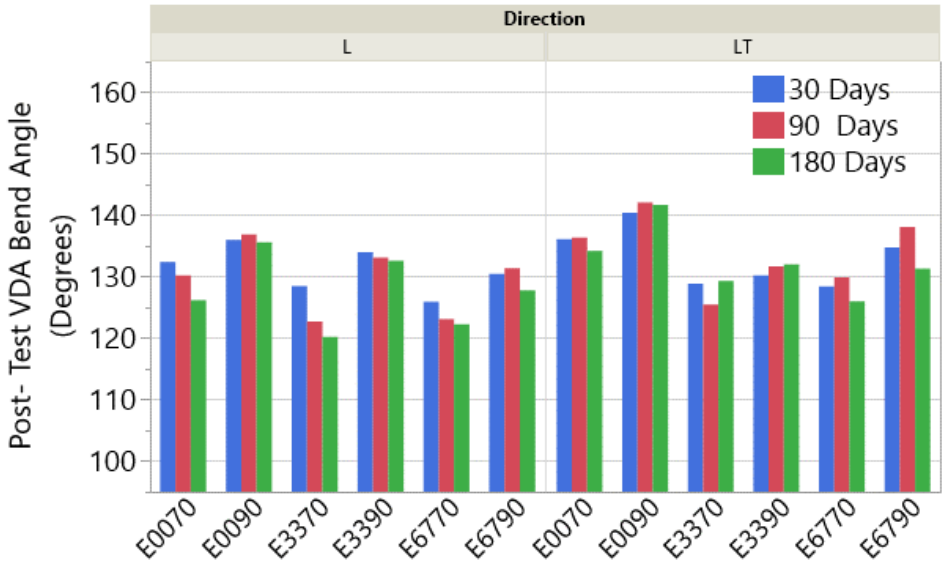

Figure 29: VDA Bend Test Results of Equivalent Strength Samples, Tested at 30 Days, 90 Days, and 150 Days of Natural Age. Labeled Direction indicates the direction in which were cut.

4.0 Discussion

4.1 Microstructure

Given that the formability and mechanical properties of automotive aluminum alloys are strongly sensitive to the alloy microstructure, which is similarly sensitive to secondary phase character and distribution, it is useful to first understand the variation in these phases. To provide a baseline expectation for the constituent phases present in each composition, proprietary software was used to predict the volume fraction of constituent particles that would be present under equilibrium conditions. As shown in **Table 11**, increases in iron and manganese content were predicted to increase the levels of these insoluble phases, with β-Al_9Fe_2Si being the dominant insoluble phase in all samples. Additionally, as manganese content increased, α-phase ($Al_{12}(Fe, Mn)_3Si$) emerged as a significant phase with a predicted volume percentage of 0.11% for the 67% scrap alloy composition. Experimentally observed constituent levels were higher than predicted quantities, but both followed a common trend of linearly increasing constituent with increasing recycle content. Note that dispersoid phases were not quantified using SEM and therefore are not included in the observed constituent area % shown in **Table 11**. Similarly, though only 70% and 90% samples were used for phase quantification, quantities of insoluble phases are not expected to differ significantly with cold work.

Table 11: Predicted and observed quantities of insoluble phases in 6XX0, 6XX1, and 6XX2.

Alloy	Fe	Mn	Predicted Al12(Fe, Mn)3Si/ α (vol. %)	Predicted Al9Fe2Si/ β (vol. %)	Observed Constituent (area %)
6XX0	0.13	0.07	-	0.28	0.368
6XX1	0.30	0.09	-	0.69	0.885
6XX2	0.40	0.16	0.11	0.92	1.139

Figure 30 summarizes the experimentally observed evolution in constituent particle metrics as a function of the summed iron and manganese content. These results quantitatively demonstrate that increasing additions of iron and manganese content, as would expected from the addition of recycle content, increases the area fraction and size of constituent particles in a nearly linear manner. Such a behavior is likely tied predominantly to an effect of Fe content; such a postulation is supported by the linear increase in particle area fraction as a function of Fe content in **Figure 31**. However, while a rapid increase in the particle number density was observed between the control composition and 33% scrap conditions, a very limited increase in this metric was noted with further scrap incorporation. This observation indicates that beyond a certain level of scrap utilization, the additional iron and manganese primarily result in particle coarsening rather than nucleation of additional particles.

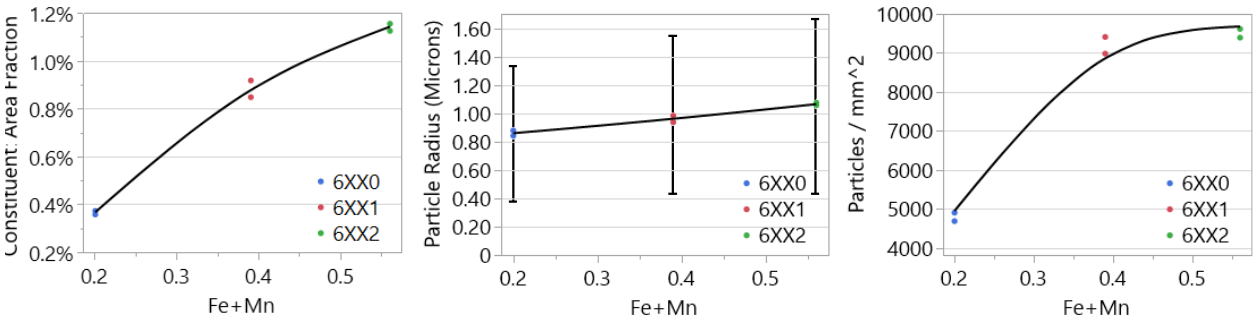

Figure 30: Constituent Particle Area Fraction, Particle Radius, and Number Density vs. Total Fe and Mn Content of 70% and 90% Cold Work Samples of 6XX0, 6XX1, and 6XX2. Error Bars Mark Particle Size Standard Deviation.

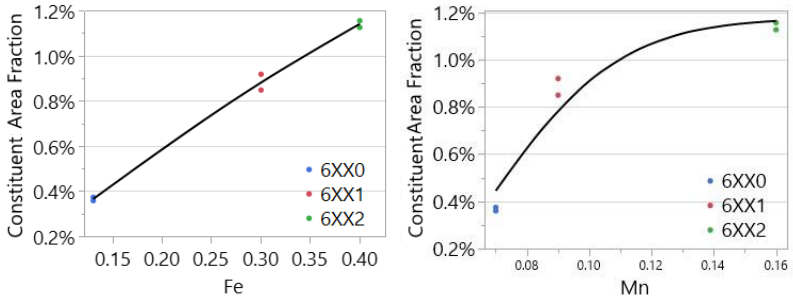

Figure 31: Constituent Particle Area Fraction vs. separated Fe, Mn Content of 70% and 90% Cold Work Samples of 6XX0, 6XX1, and 6XX2

Contrary to this trend for iron content**, Figure 31** also demonstrates that the rate of increase of constituent area fraction appears to decrease with additional manganese content. This is likely caused by the predicted formation of $Al_{12}(Fe, Mn)_3Si$ dispersoid particles in the high scrap content alloy, as indicated by the results in **Table 11**. The dispersoid phases are formed during homogenization of the ingots, and form as particles that are distinctly finer than the constituent phase particles. These particles can be seen as very fine, faint grey spots in the SEM images used to quantify constituent phases, as shown in **Figure 32**. Despite being visible in these images, even if just barely, the size of these particles makes them unlikely to be detected by the software used

to quantify constituent phase particles, likely explaining the apparent missing constituent phase in high scrap utilization alloys in **Table 11**.

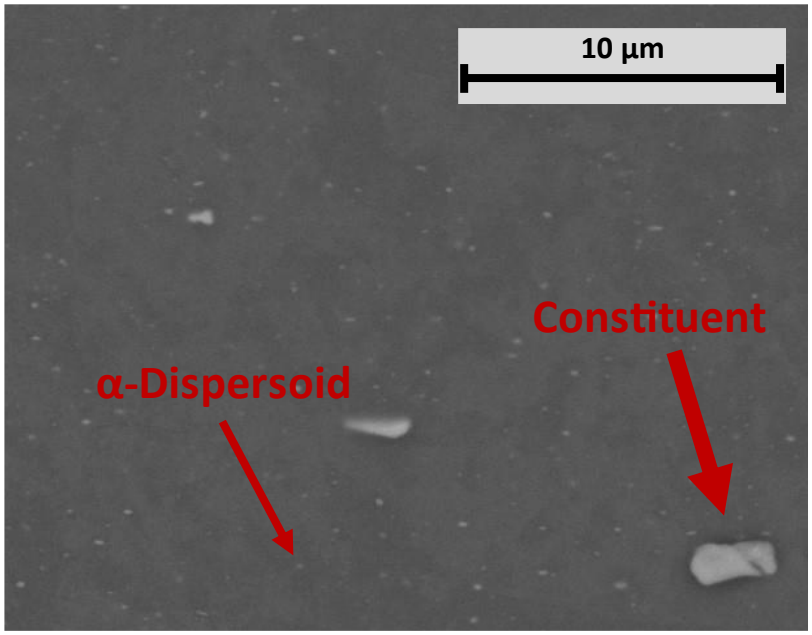

Figure 32: Magnified SEM Image of 6XX2 with α Dispersoid and Constituent Phases Labeled

One notable impact of this variation in constituent phase characteristics due to recycling content is the subsequent effect on the achieved grain size, previously shown in **Figure 18**. This effect would be expected to manifest as follows. As constituent phase volume fraction increased with recycle content, the average particle size also increased but remained within the ideal range of 0.5-2.0 µm for particle-stimulated nucleation [14], which would act to promote grain refinement. However, since number density was not observed to increase at the same rate as recycle content, the particle-stimulated nucleation effect would be expected to trail off as iron and manganese levels increased. Additionally, previous work has indicated that manganese may "neutralize" some of the iron via the formation of α-phase dispersoids, $Al_{12}(Fe, Mn)_3Si$, over β-Al_9Fe_2Si constituent [11]. Though dispersoids can cause particle-stimulated nucleation, these

particles fall below the ideal size range for such effects and, since these particles also consume iron, the increased Mn likely contributes to the decreasing particle-stimulated nucleation efficiency for the 67% scrap composition.

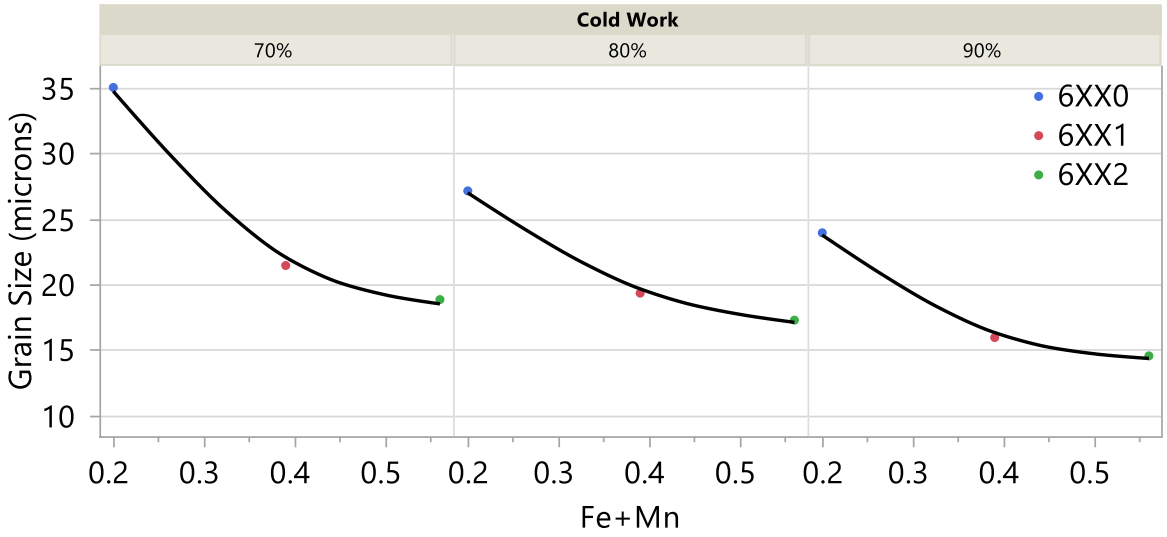

Figure 33: Number Weighted Grain size vs. Combined Fe and Mn content by Cold work Percentage.

Figure 33 confirms the impact of these simultaneous effects (increasing particle size, but saturating particle number) from increasing iron and manganese on the grain size evolution as a function of cold work. Specifically, the grain size is shown to strongly refine for all cold work levels between the control composition (6XX0) and 33% scrap composition (6XX1), but only modestly refines further with the addition of more scrap content (6XX2). Additionally, despite additions of Fe and Mn leading to decreased grain size at every cold work level, this impact was greatest in the 70% cold work samples. This is to be expected given the 70% cold work samples would have the lowest level of dislocations to act as grain nucleation sites, therefore increasing the effect of additional constituent particle-stimulated nucleation.

In addition to impacting the grain size, it was also likely that increased constituent particle fraction in the scrap alloys also led the observable precipitate phase (Mg_2Si) to generally decrease with increasing recycle content. This likely occurs due to the combination of targeting lower residual Mg_2Si in the higher scrap alloy and the consumption of silicon by constituent and dispersoid phases due to the higher presence of iron and manganese. However, the difference in residual Mg_2Si between the 70% and 90% cold work samples was much larger than expected, suggesting an important impact of unintended variation in temperature during hot rolling (**Table 9**). When designing the rolling practice for each alloy, the number of reheat cycles was kept the same between all conditions to keep the processing as uniform as possible. Despite this effort, the 90% cold work samples contained much coarser Mg_2Si than the 70% cold work samples. This is likely due to the larger hot-band gauge of the 90% cold work samples, which would have retained temperature much better than the thinner hot-band material of the 70% cold work samples and subsequently facilitated higher levels of Mg_2Si coarsening during hot rolling. Once coarsened, this Mg_2Si was difficult to dissolve during heat treatment due to the short duration of the soak above the Mg_2Si solvus temperature. If this study were to be repeated, it would likely be best to reach the hot-band gauge in the minimum number of passes for each cold work percentage rather set the number of passes and reheat cycles. This would likely have led to more similar levels of coarsening across all samples.

4.2 Mechanical Testing

Given the strong relationship between strength and local formability of these alloys, equivalent strength samples were viewed as imperative for determining the impact of increased recycle content on alloy performance. In all cases, the yield strength decreased with increasing scrap usage, as was also the case with "peak strength" conditions. As previously detailed in **Equation 1**, the model used to determine heat treatment times was based on alloy, cold work, and heat treatment duration. These factors were chosen to capture each of the four primary strengthening methods for Al-Mg-Si alloys. Solid solution strengthening and precipitation hardening were accounted for via alloy composition and normalizing all samples to ten days natural age. Grain size control was accounted for by alloy and cold work percentage while work hardening was kept at zero for all samples due to the use of a solution treatment prior to the onset of natural aging. However, one factor missing from this equation was a cross term between alloy and cold work to account for the decreasing impact of mechanical grain refinement with increasing scrap usage, which Section 4.1 revealed to be significant. If this study were to be duplicated, using grain size measurements, rather than cold work percentage, likely would have provided a more accurate model for calculating strength. These strength differences notwithstanding, targeting equivalent strength for all alloy and cold work combinations did result in a narrower range of strength values and are therefore of value for discussing differences in material performance.

First and foremost, all equivalent strength samples were shown to be capable of meeting Ford tensile specification requirements through 180 days of natural aging, as shown in **Table 12**. However, the 80% and 90% cold work samples of 6XX2 (E6780 and E6790) and 70% cold work samples of 6XX1 and 6XX2 (E3370 and E6770) would likely experience higher than acceptable

rates of failure to achieve the uniform elongation and r-value requirements, respectively, due to their proximity to the minimum requirements. In a plant setting, it is possible that the Mg_2Si present in all conditions, particularly those with higher cold work, would be decreased due to the differences in plant hot rolling schedules, which would slightly improve elongation. However, the elongation performance of the 6XX2 composition remains distinctly lower than the control alloy and it is not clear that even plant-processed 6XX2 would be sufficiently improved to regularly meet the Ford specification.

Table 12: 6XX0, 6XX1 and 6XX2 vs Ford WSS-A175-A2 Specification Limits. Properties listed are the range of values from all cold work levels.

	Ford WSS-A174-A2	6XX0	6XX1	6XX2
TYS (MPa)	105-145	119-133	109-130	112-126
UTS (MPa)	200-270	241-259	230-259	234-255
UEL (%); min	19	20.4-23.9	19.1-22.6	19.1-21.8
r value @ 10%; min	0.5	0.585-0.830	0.525-0.700	0.510-0.660

These data confirm Research Hypothesis #1, which stated that the highest scrap level alloy (6XX2) would have sufficiently reduced global formability to challenge the Ford specification requirements. In addition to the requirements of Ford's specification higher scrap usage was shown to lead to decreases in total elongation and strain hardening exponent. Though not required by Ford specification, many other OEMs define limits for these properties, and both are considered valuable indicator of formability. Overall, the decrease in the tensile properties which indicate global formability would imply that 6XX2 would likely experience failure during part stamping and is likely not suitable for application requiring extensive forming, regardless of hemming requirements. However, these data also support Research Hypothesis #2, which stated that the intermediate scrap alloy composition would be able to generally meet the Ford specification

requirements with modifications in alloy processing. As demonstrated by the results of this effort, increasing the amount of cold work for 6XX1 results in uniform elongation and plastic strain ratio values that are adequate for this Ford specification.

Interestingly, additions of iron and manganese seemed to have significantly more impact to total elongation measured transverse to the rolling direction than elongation measured longitudinally. This is shown below in **Figure 34**. This effect does not appear to be as severe when comparing the uniform elongation of samples and is nonexistent for the measured r and n values. Additionally, transverse elongation was found to be lower in all samples, including the control. This relationship is not typically seen in plant-produced material, as is evident in the listed properties for AA6022 sheet [2].

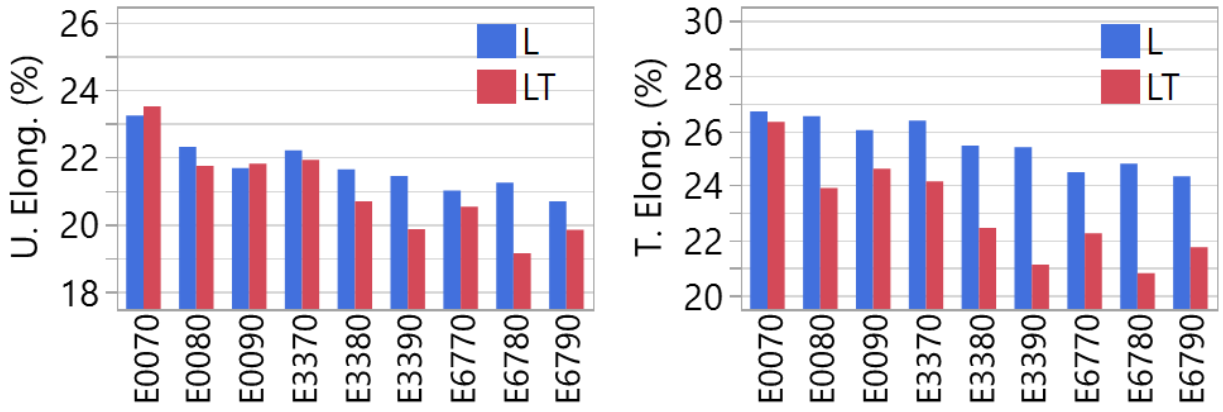

Figure 34: Uniform Elongation and Total Elongation of Equivalent Strength Lots Showing Large Impact of Increased Scrap Usage on Total Elongation

One possible explanation of this phenomena is an increase in outside gauge length (OGL) failures in the transverse direction. OGL failures occur when the tensile breaks outside of the measured area of the specimen. This results in an artificially low elongation, which if severe

enough, can result in lower measured uniform elongation. A hallmark of OGL failures is a low difference between the total and uniform elongation, which was observed in all LT specimens of the 6XX1 and 6XX2 compositions. **Figure 35** shows the stress strain curves of various in the E3370-LT specimen. Samples with an OGL failure present a sharp, vertical end to the stress- strain curve. These failures are more likely when properties are not uniform across the length of the tensile specimen. This property variation may have been caused by uneven cooling on at the edge and center of the sheet during hot rolling, resulting in faster edge cooling and potentially causing slightly uneven Mg_2Si precipitation across the transverse direction of the sheet.

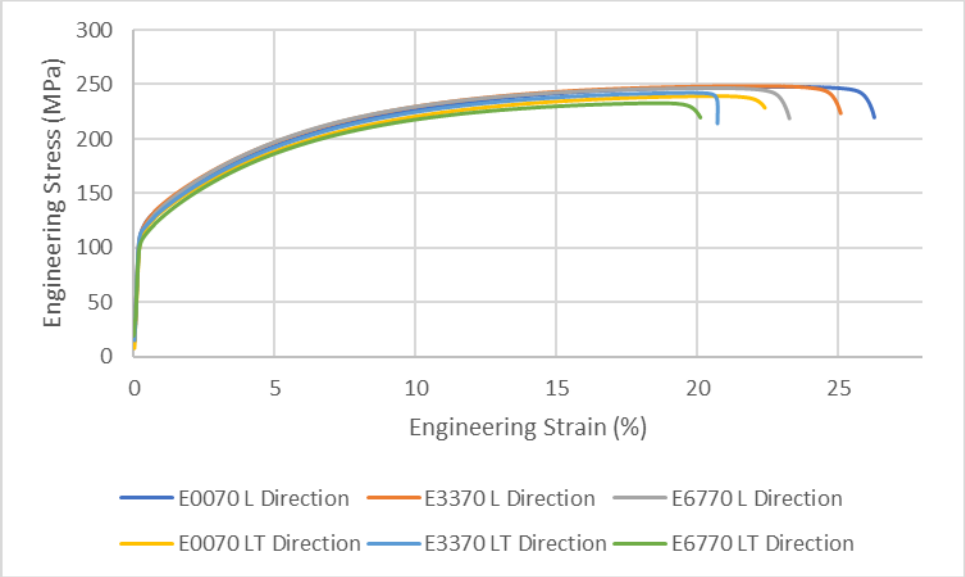

Figure 35: L and LT Stress Strain curves from Equivalent Strength Lots with OGL failure of E3370 LT Specimen

Another potential explanation of the lower observed differences between the total and uniform elongation in the LT direction relative to expectations could be differences in texture between lab-made and plant-made sheet. While texture was not explicitly explored in this study and is the subject of future work, texture would be modified since each of the heat cycles used

during lab rolling effectively acts as an anneal, causing partial recrystallization and coarsening of precipitate phases. Given the increased grain nucleation with increased constituent, it is likely that these differences would be more severe in alloys with higher recycle content. When coupled with the lower overall ductility of the high recycle content, the increased OGL likelihood and textural variation of lab made sheet provide a likely explanation for the lower LT elongation in the higher recycle content alloys.

Evaluating the alloys purely based on performance in the flat hem test, increased scrap usage notably improved hem performance, even in equivalent strength conditions. In fact, the control alloy was found to surprisingly struggle to meet the Ford specification requirement, even at 30 days natural age in both the equivalent and peak strength condition. Though control alloy samples were observed to have higher strength, this is not likely the sole explanation for the improved performance of the higher scrap alloys. For example, comparing the 30-day results of the control alloy to 180-day results of the 67 % scrap alloy, the higher scrap alloy still outperformed the control samples. Instead, it is speculated that the grain refinement effect (**Figure 33**) from the additional iron and manganese is the cause for this improved performance for the scrap-bearing alloys. As was also demonstrated by the effect of increasing cold work irrespective of scrap content, smaller grains unquestionable lead to an improvement in flat hem performance across all tested conditions in this study. While the 6XX2 composition typically performed the best in hemming, it is notable that the 6XX1 composition also appears to be capable of meeting the Ford requirements at higher levels of cold work. Given the superior tensile properties of 6XX1 (**Table 12**), the use of 80% or 90% cold work would appear to meet all mechanical property requirements of the Ford specification. Notably, lab processes often result in inferior bend properties, regardless of alloy composition, and it is likely that plant-produced sheet of each composition would pass a

hem test at 30 days of natural aging at all cold work levels. However, it is likely that the trends seen in lab-produced material would hold true in plant fabricated sheet and higher cold work 6XX1 would likely remain the best option for meeting Ford specification requirements.

Even though both high scrap usage alloys outperformed the control alloy across the board, it is clear when viewing the data that the test is not perfect. Notably, the 90-day samples performed dramatically worse than both 30- and 180-day results for many of the equivalent strength conditions. More than a true indicator of material performance, this is almost certainly an indicator of the variability of the test and material. Since the inner radius of the down flange is adjusted based on nominal material gauge, even slight variations in gauge (certainly possible with lab-rolled material) can have an impact on hem performance. For this reason, VDA bend results were also considered when evaluating hem performance. This test not only gives an objectively quantitative measure of material performance, but results are also less sensitive to geometrical differences between samples. As discussed in Section 3, VDA bend results were largely contrary to hem results with respect to alloy performance (e.g., the good performance of the control composition), though the trend of improving bend performance with increased cold work held true for both VDA and flat hem tests. One possible explanation of this is the increased level of pre-strain prior to the VDA bend test. Since the hem and VDA experiments are evaluations of both local and global formability, higher levels of pre-strain will during the VDA test will intrinsically favor alloys with improved global formability.

Overall, these uniaxial mechanical testing and formability measurements imply that automotive applications requiring moderate levels of global formability and high levels of local formability could be achieved with alloys containing iron and manganese levels higher than what alloys such as AA6022 currently allow. This of course means that moderately increased scrap

usage in alloys designed for such applications has the potential to improve overall material performance. This impact is seen across cold reduction levels, though the positive impacts of increased scrap usage are most apparent in products with moderate levels of cold work. While the 33% scrap utilization alloy seemingly performed best among its peers, it is likely that the levels of scrap used in this alloy would not be ideal for applications requiring higher levels of global formability prior to hemming. Instead, alloys with this level of scrap usage would be better suited for use in hemming applications with more limited forming, such as body side outer panels or outer door panels in vehicles that lack aggressive styling.

5.0 Conclusions

This study set out to determine the impact of increased recycle content on microstructure and mechanical properties in wrought Al-Mg-Si alloys. The composition of the recycle content used was a 50-50 mixture of Ford high and low copper Al-Mg-Si scrap streams with a small amount of extra iron to reflect contamination from rivets, tooling, etc. The three alloys evaluated in this study, 6XX0, 6XX1, and 6XX2 had escalating recycle content with 0%, 33%, and 67% scrap utilization, respectively. The resulting compositions had varying Fe and Mn levels with a base composition targeting the properties required by Ford WSS-A175-A2, a low copper Al-Mg-Si grade used for applications requiring limited hemming capabilities. Iron levels were varied between 0.13 wt.% in the control alloy, 0.3 wt.% in the moderate scrap alloy and 0.4 wt.% in the high scrap alloy. Manganese was varied between 0.075 wt.%, 0.09 wt.%, and 0.16 wt.% in the high scrap alloy. These alloys were evaluated across three levels of cold reduction, 70%, 80% and 90%, to produce varied grain size and structure, allowing the alloys to be compared across a range of typical processing methods.

As expected, the increased recycle content resulted in an increase in insoluble phases. This relationship was largely linear, though higher levels of manganese seemed to result in a higher level of dispersoid phases, which were not quantified by the methods employed in this study. Higher levels of insoluble phases were linked with the presence of smaller grains, likely caused by the effects of particle-stimulated nucleation.

Overall, increased recycle content was observed to have negative impacts on the mechanical properties that serve as indicators of global formability, elongation, plastic strain ratio,

and strain hardening exponent. This trend was observed uniformly across all levels of cold work. Despite decreased global formability, the moderate recycled content composition (6XX1) was able to meet all aspects of Ford WSS-A175-A2 specification requirements. However, the recycle content of the high scrap alloy (6XX2) proved too high to meet Ford tensile specification requirements due to decreased elongation and plastic strain ratio.

Ford flat hem and VDA bend experiments were used to evaluate the local formability performance of each alloy condition. The results of the evaluation of the hemming capabilities of each alloy were mixed, with alloy performance varying with test methods. The higher scrap alloys showed improved performance versus the control composition during flat hemming, while the control alloy outperformed higher scrap alloys in the VDA bend experiment. The improved bend performance of the moderate and high recycle content alloys in the flat hem test is most likely attribute to the decreased grain size of these alloys driven by the change in constituent particle characteristics. The difference in performance between the flat hem and VDA bend test is believed to be due to the higher levels of pre-strain in the VDA bend test biasing the results towards alloys with improved global formability metrics, such as the control composition. Because Ford lists no specification limit for VDA bend performance, the Ford flat hem test was considered the benchmark for alloy performance. The 80% and 90% cold work samples of 6XX1 meeting passing the Ford flat hem test through 180 days natural age. All 6XX2 samples were able to pass this test through 180 days, while only 90% cold work samples of the control alloy consistently passing the hem test.

Ultimately, moderate levels of scrap utilization were shown to have a tolerable impact on tensile properties, while seemingly improving bend performance during hemming experiments. The 80% and 90% cold work conditions for this alloy composition were the only tested lots to

consistently met all Ford requirements through 180 days of natural aging. These results were consistent with the governing hypotheses of the experiment, demonstrating that moderate levels of recycled content can be used to improve overall performance, while higher levels of scrap utilization would likely have too strong of an impact on global formability to meet current tensile property requirements.

6.0 Future Work

The findings of this study imply that there is likely room for higher recycle content alloys in the automotive marketplace. From an industry perspective, future efforts should focus on optimizing the alloy composition for performance using a targeted scrap usage threshold, rather than to simply evaluate the performance of an alloy with a set scrap utilization target. Additional optimization of the Fe and Mn content in Al-Mg-Si alloys is likely to result in improved hem performance and sustainability. Furthermore, each of the alloys in the current study occupied the upper end of the allowable strength range by the Ford specification. Modifications of Mg, Si, and Cu content likely would result in improved properties as excessive strength or undissolved Mg_2Si can both act to decrease ductility and formability.

From a more academic perspective, one of the greatest causes of unintended variation in this study was the use of laboratory-scale processing. For example, the need for re-heat cycles during hot rolling to counteract the more rapid cooling rates of the lab-scale ingots relative to what would occur in a plant setting will have an impact on developed microstructure. Similarly, the variation inherent in laboratory-scale rolling can cause important variations in Mg_2Si morphology and subsequently introduce differences in crystallographic texture. These challenges underscore the need for further understanding of how recycle content impacts through-process texture evolution. Such insights could then be leveraged to improve thermomechanical processing of high recycle content alloys as well as help explain some of the unexpected results in the present study.

7.0 Bibliography

[1] Aiura, T., & Sakurai, T. (2010). *Development of Aluminum Alloys and New Forming Technology for Automotive Parts*.

[2] ALCOA ALLOY 6022. (2009). Alloy Digest, 58(4). https://doi.org/10.31399/asm.ad.al0421

[3] Burger, G. B., Gupta, A. K., Jeiirey, ? W, & Lloyd, D. J. (1995). *Microstructural Control of Aluminum Sheet Used in Automotive Applications*.

[4] Choate, W. T., & Green, J. A. S. (2003). U.S. energy requirements for aluminum production: Historical perspective, theoretical limits and new opportunities. *TMS Annual Meeting*.

[5] Das, S. K., Green, J. A. S., & Kaufman, J. G. (2007). The development of recycle-friendly automotive aluminum alloys. In *JOM* (Vol. 59, Issue 11). https://doi.org/10.1007/s11837-007-0140-2

[6] Dewang, Y., & Sharma, V. (2019). A study on sheet metal hemming process. *Materials Today: Proceedings*, *27*. https://doi.org/10.1016/j.matpr.2019.09.074

[7] Engler, O., Marioara, C. D., Hentschel, T., & Brinkman, H. J. (2017). Influence of copper additions on materials properties and corrosion behaviour of Al–Mg alloy sheet. *Journal of Alloys and Compounds*, *710*. https://doi.org/10.1016/j.jallcom.2017.03.298

[8] Furu, T., Telioui, N., Behrens, C., Hasenclever, J., & Schaffer, P. (2010). Trace elements in aluminium alloys: their origin and impact on processability and product properties. *Proceedings of the 12 ICAA*, 282–289. http://www.icaa-conference.net/ICAA12/pdf/KL-10.pdf

[9] Hatch, John E. (1984). Aluminum: Properties and Physical Metallurgy - ASM International. In *Aluminum Science and Technology*.

[10] Hirsch, J. (2006). *Virtual fabrication of aluminium products : microstructural modeling in industrial aluminum production*. Wiley-VCH.

[11] Ji, S., Yang, W., Gao, F., Watson, D., & Fan, Z. (2013). Effect of iron on the microstructure and mechanical property of Al–Mg–Si–Mn and Al–Mg–Si diecast alloys. Materials Science and Engineering: A, 564, 130–139. https://doi.org/10.1016/j.msea.2012.11.095

[12] Kaffl, R. (2023, December 28). *FORD F-SERIES: AMERICA'S BEST-SELLING TRUCK FOR 47 YEARS AND COUNTING*. Ford Media Center.

[13] Khan, M. H., Das, A., Li, Z., & Kotadia, H. R. (2021). Effects of Fe, Mn, chemical grain refinement and cooling rate on the evolution of Fe intermetallics in a model 6082 Al-alloy. Intermetallics, 132, 107132. https://doi.org/10.1016/j.intermet.2021.107132

[14] Kishchik, M. S., Mochugovskiy, A. G., Cuda, M., Kishchik, A. A., & Mikhaylovskaya, A. v. (2023). Particle Stimulated Nucleation Effect for Al-Mg-Zr-Sc Alloys with Ni Addition during Multidirectional Forging. Metals, 13(8), 1499. https://doi.org/10.3390/met13081499

[15] Laughlin, D. E., Miao, W. F., Karabin, L. M., & Chakrabarti, D. J. (1998). Effects of Cu and Mn content and processing on precipitation hardening behavior in Al-Mg-Si-Cu alloy 6022. *TMS Annual Meeting*.

[16] Mracna, C. (2014). *Engineering Material Specification: Aluminum Alloy, Sheet, Heat Treatable, Enhanced Bake Response.* www.gma.ford.com

[17] Mracna, C. (2014). *Flat Hem Test Procedure for Aluminum Alloy Sheet.* www.gma.ford.com

[18] Mracna, C., Sinclair, L., & Wetekamp, L. (2022). *Engineering Material Specification, Heat Treatable, Structural, High Strength, Thick Gauge*. www.gma.ford.com

[19] New sorting system for separating aluminium alloys. (2016, October 17). Recycling-Magazine. https://www.recycling-magazine.com/2016/10/17/new-sorting-system-for-separating-aluminium-alloys/

[20] Raabe, D., Ponge, D., Uggowitzer, P. J., Roscher, M., Paolantonio, M., Liu, C., Antrekowitsch, H., Kozeschnik, E., Seidmann, D., Gault, B., de Geuser, F., Deschamps, A., Hutchinson, C., Liu, C., Li, Z., Prangnell, P., Robson, J., Shanthraj, P., Vakili, S., … Pogatscher, S. (2022). Making sustainable aluminum by recycling scrap: The science of "dirty" alloys. Progress in Materials Science, 128, 100947. https://doi.org/10.1016/j.pmatsci.2022.100947

[21] Shang, J., Wilkerson, L., & Hatkevich, S. (2011). Hemming of aluminum alloy sheets using electromagnetic forming. *Journal of Materials Engineering and Performance*, *20*(8). https://doi.org/10.1007/s11665-011-9988-y

[22] VDA Empfehlung 238-100 / VDA Recommendation 238-100 Plättchen-Biegeversuch für metallische Werkstoffe Plate bending test for metallic materials VDA 238-100. (2017). www.vda.de

[23] Zhu, Y., Chappuis, L. B., de Kleine, R., Kim, H. C., Wallington, T. J., Luckey, G., & Cooper, D. R. (2021). The coming wave of aluminum sheet scrap from vehicle recycling in the United States. *Resources, Conservation and Recycling*, *164*. https://doi.org/10.1016/j.resconrec.2020.105208